Retreat of the Great Escarpment of Madagascar from Geomorphic Analysis and Cosmogenic ^{10}Be Concentrations

Y. Wang[1], S. D. Willett[1], D. Wu[2] , N. Haghipour[1], M. Christl[3]

[1]ETH Zurich, Department of Earth Sciences, Sonneggstrasse 5, 8092 Zurich, Switzerland.

[2]China Geological Survey, Shengyang Center, Huanghe North Street 280, 110034 Shenyang, China.

[3]ETH Zurich, Department of Physics, Laboratory of Ion Beam Physics, Otto-Stern-Weg 5, 8093 Zurich, Switzerland.

Corresponding author: Yanyan Wang (yanyan.wang@erdw.ethz.ch)

Key Points:

- Presentation of new detrital cosmogenic ^{10}Be data that systematically covers the great escarpment of eastern Madagascar.
- Erosion rates inferred from ^{10}Be concentrations are 9.7 m/Ma to 27 m/Ma, systematically vary among distinct morphological zones.
- Escarpment retreat rates from ^{10}Be concentrations are 182 m/Ma to 1886 m/Ma, consistent with evidences for captures and divide migration.

Abstract

The eastern margin of Madagascar has a prominent relief change from the flat coastal plain to the low-relief high plateau, characterizing a typical great escarpment topography at a passive margin. A quantification of the spatial distribution of erosion rates is necessary to understand the rate of landscape evolution. We present catchment-averaged erosion rates from detrital cosmogenic ^{10}Be concentrations, systematically covering distinct morphological zones of the escarpment. Erosion rates are differentiated across the escarpment, where the high plateau and the coastal plain are slowly eroding with an average rate of 9.7 m/Ma, and the escarpment basins are eroding faster with an average rate of 16.6 m/Ma. The Alaotra-Ankay Graben related basins have the highest erosion rate with an average rate of 27 m/Ma. The spatial pattern of erosion rates indicates a retreating escarpment landscape. Retreat rates calculated from the ^{10}Be concentrations are from 182 m/Ma to 1886 m/Ma. The rates of escarpment retreat on Madagascar are consistent with a model of a steady retreat from the coastline since the time of rifting, similar to the Western Ghats escarpment on its conjugate margin of the India Peninsula.

Plain Language Summary

Eastern Madagascar is characterized by a distinct escarpment with high relief, normally indicative of high erosion rates. We investigate this by measuring erosion rates using cosmogenic isotope concentrations in sediment derived from throughout Madagascar. We calculated erosion rates and related these to distinct geomorphic zones. The pattern of erosion rates is consistent with inland retreat of the escarpment at about 1 km/Ma. This rate is consistent with geomorphic evidence and is comparable to the conjugate margin of western India.

1 Introduction

Madagascar is one of the world's largest islands, separated from the Africa continent by the Mozambique Channel (Figure 1a). The main water divide of Madagascar follows the longitudinal axis of the island and separates drainages of the Indian Ocean from the Mozambique Channel (Figure 1b), although the topography is strongly asymmetric with eastward-flowing rivers shorter (<150 km) than westward flowing rivers (>300 km). Madagascar was at the center of the Gondwana supercontinent and was surrounded by the ancient Africa continent and the continent of the Seychelles-India (Wit, 2003). The rifting between Madagascar and Seychelles-India started between 120-92 Ma based on ages of basaltic intrusions and dikes at the eastern margin of Madagascar (Torsvik et al., 1998; Melluso et al., 2005). Final separation is dated to the late Cretaceous from volcanic provinces and the oldest seafloor magnetic anomaly in Indian Ocean, Chron 34 (~84 Ma) (Eagles and Hoang, 2014), and is limited to being older than the Deccan volcanic province eruption at the western margin of the India peninsula (~65 Ma) (Collier et al., 2008). Rifting between Madagascar and Seychelles-India has formed the paired mountain ranges along the coast at the conjugate margins of eastern Madagascar and western India (Gunnell and Harbor, 2008).

Unlike the west margin where the central high plateau gradually flattens into the coastal plain, the east margin is characterized by an escarpment where the relief abruptly increases from the flat coastal plain to the high flat plateau, with the water divide sitting at or near the eastern margin of the highlands. The topography of the conjugate margin of western India, the Western Ghats, is similar and is well-recognized as a great escarpment (Mandal et

al., 2015; Gunnell and Harbor, 2010; Gunnell and Harbor, 2008), but Madagascar has not received the same attention. In fact, several studies of the Madagascar topography interpret the high-relief, steep escarpment zone to be river knickpoints formed by recent uplift rather than rift-related escarpments (Stephenson et al., 2021; Stephenson, 2019; Roberts et al., 2012).

There is some evidence for Cenozoic uplift of Madagascar. A major erosional unconformity from Oligocene to Miocene (30-16 Ma) is revealed from offshore wells on the west margin (Delaunay, 2018). This unconformity is likely regional given that Oligocene sediment is also missing on land (Tucker et al., 2012). Eocene to Pleistocene marine/shoreface sediment crops out at the western and southern marginal areas (Tucker et al., 2012; Stephenson et al., 2019) and are currently up to 300 meters above sea level. The Cenozoic sedimentary rock indicates uplift and westward tilting of Madagascar (Delaunay, 2018). Delaunay (2018) interpreted stepped erosional surfaces on Madagascar as indicating two major uplift episodes of the central plateau, from the late Cretaceous to early Paleogene (94-66 Ma) and from the Oligocene to Miocene (34-5Ma).

The high central plateau, which defines the western boundary of the escarpment mountain range, is in a state of isostatic equilibrium, except in the northernmost part of the island where the relatively high topography can't be purely supported by its crustal thickness (Andriampenomanana et al., 2017). The northernmost part of Madagascar is characterized by slow shear-wave velocities in the uppermost mantle (Andriampenomanana et al., 2017; Pratt et al., 2017). The low shear-wave area coincides with the Neogene to Pleistocene volcanism. Upwelling, hotter mantle in the northernmost part of Madagascar is interpreted to be responsible for Pleistocene uplift of the nearby coastal region, where uplifted late Pleistocene-Holocene coral reefs and marine terrace deposits indicate recent uplift (Stephenson et al., 2019).

Rates of erosion provide important constraints on the landscape evolution. Apatite fission track ages (AFT) and (U-Th)/He ages on the coastal plain of the eastern margin of Madagascar are between 68 Ma to 400 Ma (Emmel et al., 2012), rarely significantly younger than the break-up age, although cooling ages are older on the central high plateau than on the eastern coastal plain suggesting some effects of rifting (Emmel et al., 2012). However, these ages are too old and imprecise to distinguish between a retreating escarpment scenario or a static, or downcutting topography since rifting. Globally, this is typical that thermochronometry is unable to resolve erosion rates with the precision needed to constrain landscape evolution models. Short-term erosion rates are slow (~10 m/Ma) on the high plateau according to sparsely published erosion rates from detrital cosmogenic nuclide (DCN) ^{10}Be concentrations (Cox et al., 2009), similar to reported erosion rates for the plateau hinterland of other passive margins (e.g. the Deccan plateau hinterland of the Western Ghats (Mandal et al., 2015); the plateau of the southeastern Australia escarpment (Godard et al., 2019).

In this paper, we address the landscape evolution of Madagascar and the formation of the eastern escarpment through a systematic study of erosion rates determined by detrital cosmogenic nuclide ^{10}Be concentrations, with a focus on southeast Madagascar. Regional patterns of erosion rates and the relationship to the morphology of the landscape are studied. In particular, we evaluate evidence for the retreat of the escarpment and measure its rate, making a comparison with the conjugate escarpment of the Western Ghats, India.

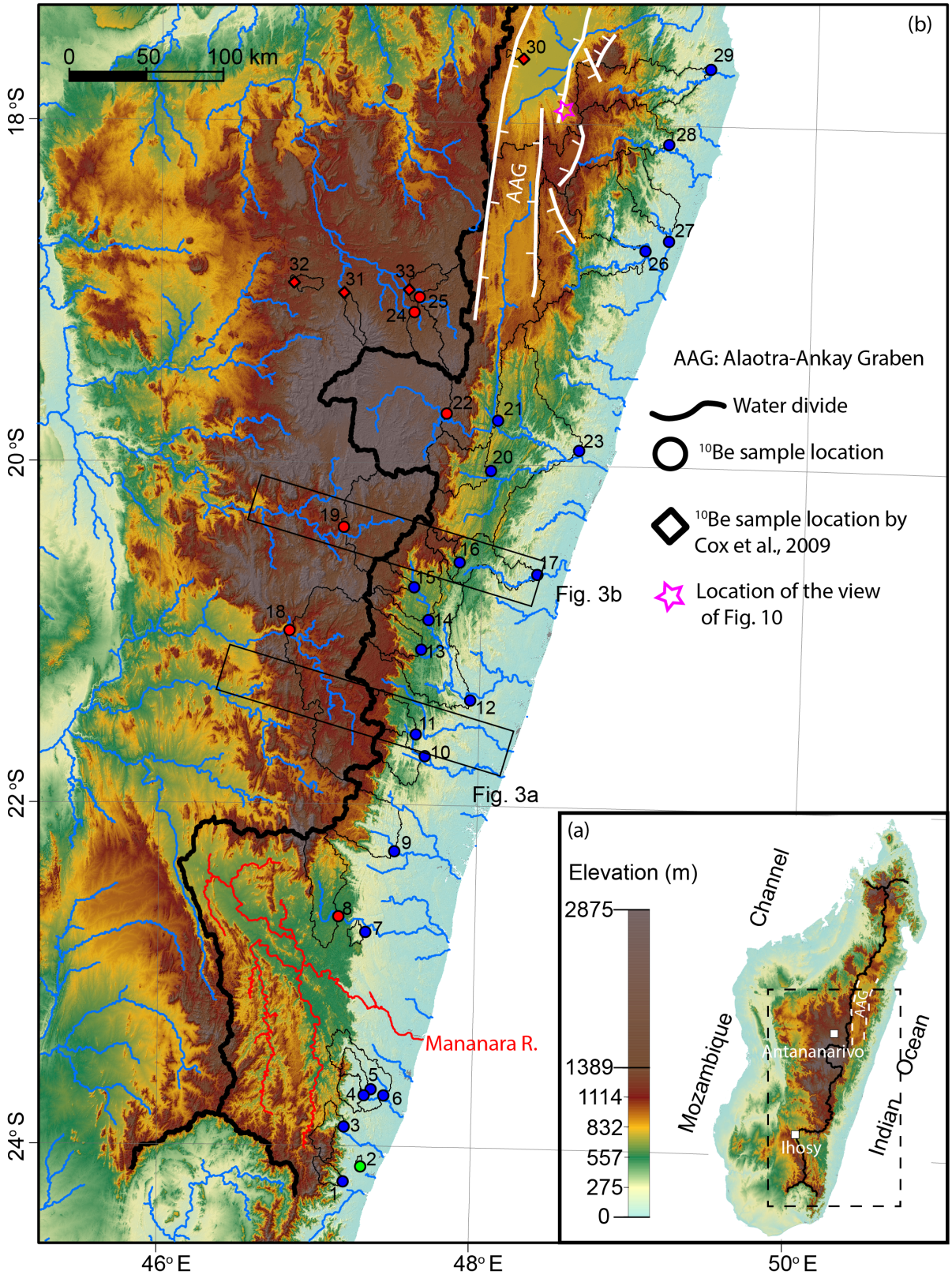

Figure 1. (a) The geographic setting of Madagascar. The black dashed box indicates the study area. (b) SRTM-90 meter digital elevation model (Jarvis et al., 2008) of Madagascar showing the continental water divide, major rivers and cosmogenic nuclide ^{10}Be basins in this research. Rivers with drainage areas larger than 400 km^2 are indicated in blue. The Mananara River which we will discuss later is indicated in red. Black polygons are sampled ^{10}Be

118 catchments. ^{10}Be sampling locations are shown with circles. Basin type is color-coded: red is
119 a plateau basin, blue is an escarpment-draining basin and green is a coastal plain basin. White
120 filled diamonds are ^{10}Be samples from Cox et al. (2009). Numbers refer to basin ID used in
121 the main text and associated tables. Thick white lines are simplified normal faults from
122 Kusky et al. (2010).

123

124 **2 Study area**

125 2.1 Lithology, climate and hydrological setting

126 The geology of Madagascar can be simplified into three domains: the Precambrian
127 shield of the central and east of the island, rift-related sedimentary sequences from late
128 Carboniferous to Cretaceous in the west, Cretaceous and Neogene volcanic provinces
129 distributed across the island (Figure 2a). In our study area, Precambrian paragneiss and
130 orthogneiss dominate the central plateau, the escarpment, and the coastal plain (Figure 2a).

131 Madagascar is mostly in a tropical climate regime, but the precipitation and
132 temperature are subject to altitude, monsoon, and proximity to the coastline. The monsoon
133 moisture comes from the Indian Ocean, impacting mostly southeastern Madagascar (Scroxton
134 et al., 2017). The annual precipitation decreases from east to west, and also from north to
135 south (Figure 2b). In the study area, the eastern coastal plain and the escarpment are rainy
136 year-round, due to an orographic effect (Figure 2a and Figure 3, Ohba et al., 2016). Annual
137 rainfall in the northern portion of the high plateau is mostly from the summer monsoon
138 during November to April, whereas the southern part of the central high plateau is subtropical
139 and dry (Nassor and Jury, 1998). Paleomagnetic studies have reconstructed the paleolatitude
140 of Madagascar to be between 30°S to 40°S at Chron 34 (~84 Ma) (Schettino and Scotese,
141 2005). The northward drift of Madagascar pulled it out of subtropical latitudes to the present
142 tropical zone progressively during the Cenozoic (Ohba et al., 2016).

143

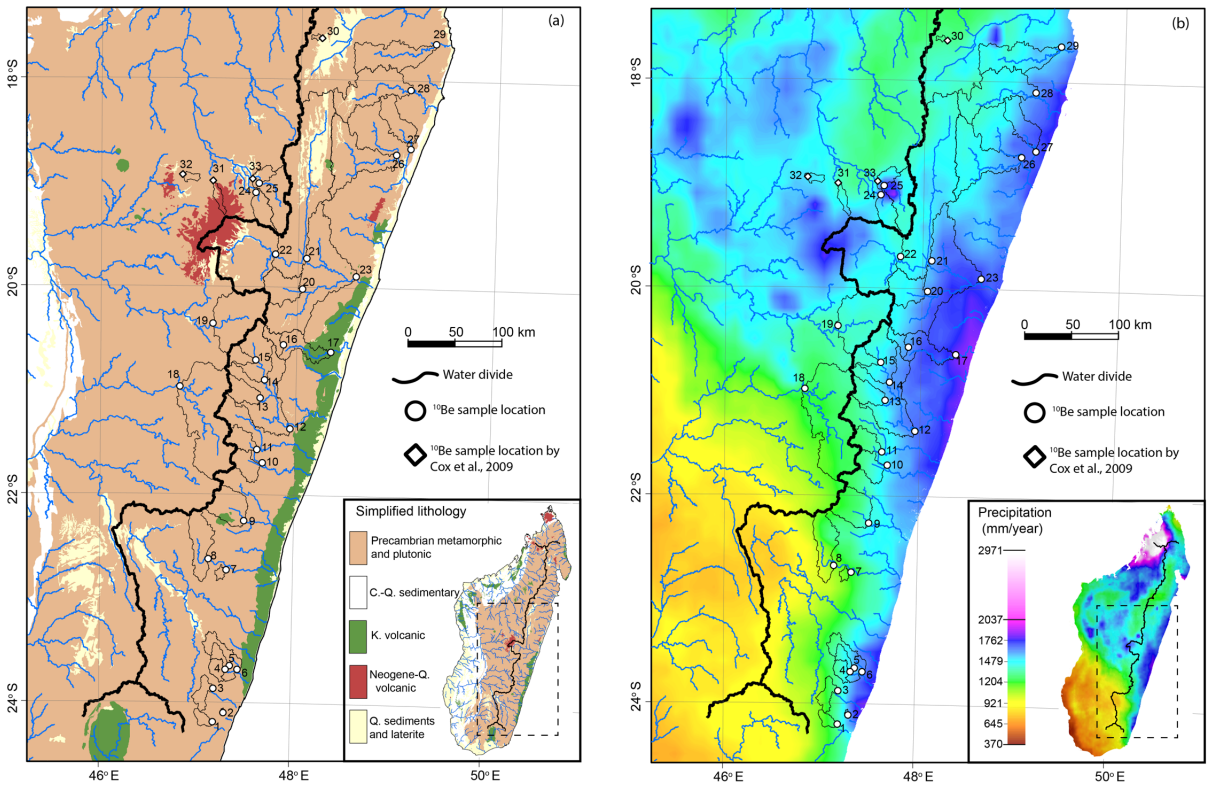

Figure 2. (a) Simplified lithology of Madagascar after the geological map from Roig et al. (2012) and lithology description from Tucker et al. (2012). (b) Average annual precipitation of Madagascar from 2014 to 2018. Raw data is from IMERGHH version 6.0. The IMERGHH version 6.0 data were provided by the NASA/Goddard Space Flight Center and PPS, which develop and compute the dataset as a contribution to GPM project and archived at the NASA GES DISC. Available at: https://pmm.nasa.gov/data-access/downloads/gpm.

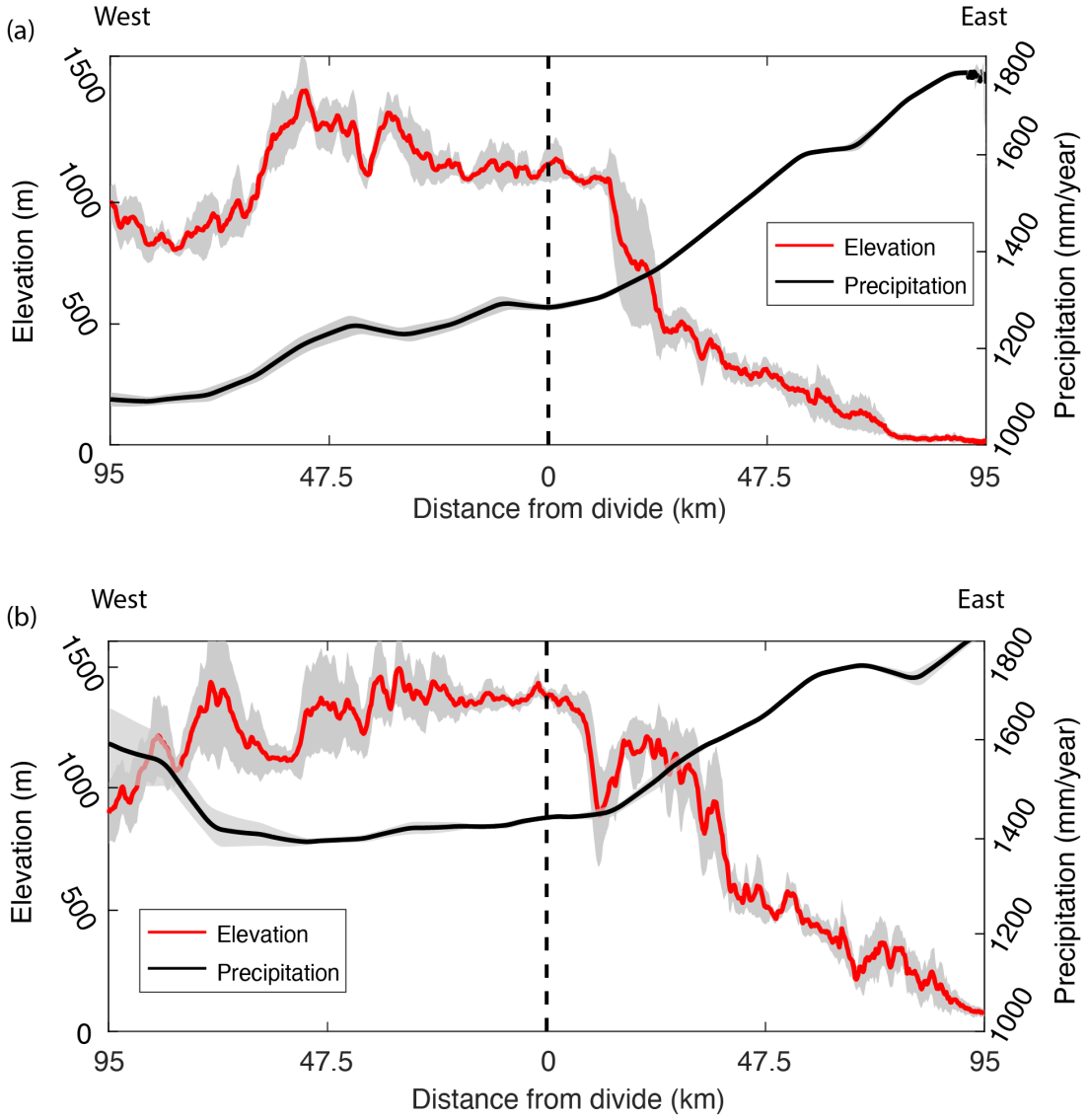

Figure 3. (a) and (b) Swath profiles across the continental water divide showing the asymmetric topography and orographic precipitation across the divide. Position of the swaths are indicated in Figure 1. Swath window is 30 km wide.

2.2 Morphology

Southeastern Madagascar exhibits three topographic domains: the low-lying coastal plain on the eastern margin, the highlands of the central plateau, and the high-relief, steep escarpment separating the two. Although the escarpment extends for the entire length of the island, in the study area, it is most clearly defined for ~500 km in southern Madagascar (Lat. 19° S-24° S) (Figure 1) where we will focus our study. The coastal plain, escarpment, high plateau landscape is also found in other passive margins, e.g. the Western Ghats of India that form the conjugate margin to Madagascar (Mandal et al., 2015), the Serra do Mar in southern Brazil (Salgado et al., 2016), as well as in the southeastern margin of Australia (Godard et al., 2019).

The steep and high-relief belt that is located between the low-lying, low-relief coastal plain and the low-relief high plateau can be regarded as a passive margin escarpment

(Gunnell and Harbor, 2010). A passive margin with a great escarpment is characterized by rapid elevation gains of hundreds of meters to over one kilometer over a relatively short distance, forming a prominent asymmetric topography (Matmon et al., 2002). In Madagascar, the escarpment has a relief of 550-2000 m in the southern Ihosy area and is 1300-2800 m in the central Antananarivo area (Figure 1). The Madagascar escarpment has similar morphology to the Western Ghats, a well-recognized great escarpment along the western margin of the India Peninsula (Gunnell and Harbor, 2008). In Madagascar, north of Lat. 19.5° S, the active Alaotra-Ankay Graben has affected the morphology of the escarpment (Gunnell and Harbor, 2008). From Lat. 19.5° S to 24° S, rivers east of the divide frequently follow the late Proterozoic-gneissic foliations, which are subparallel to the escarpment and brittle fractures that are oblique to the escarpment (Schreurs et al., 2009). High remnant escarpments, referred to as "buttes" by Gunnell and Harbor (2010), are prevalent from Lat. 19.5°S to 21.5°S (Figure 1). The coastal plain adjacent to this escarpment segment gently dips towards the Indian ocean (Figure 3b). The escarpment south of Lat. 21.5°S is lower in elevation and the buttes are also lower than equivalent features in the northern escarpment segment (Figure 1).

The asymmetry in river length across Madagascar persists after normalization for drainage area, as indicated by the normalized length parameter, χ (Figure 4) (Perron and Royden, 2013). This asymmetry is likely to be a consequence of the continental rifting which broke the pre-existing Gondwana-wide continental river network, creating a new base level for rivers which drain the bordering escarpments. The final rifting on the east coast of Madagascar set the dominant pattern with a west-migrating continental divide. Other factors such as climate, lithology and uplift rates can also affect asymmetry. The wetter climate of the east coast (Nassor and Jury, 1998) should also encourage migration of the divide to the west. Rivers on the west of the water divide flow across two distinct lithological domains, the Precambrian crystalline shield and the Mesozoic-Cenozoic sedimentary cover (Figure 2a), before joining the Mozambique Channel. The sedimentary cover is potentially softer and more erodible and evidence for this difference is evident in river profiles. Rivers on the east of the divide carve exclusively into the Precambrian crystalline basement.

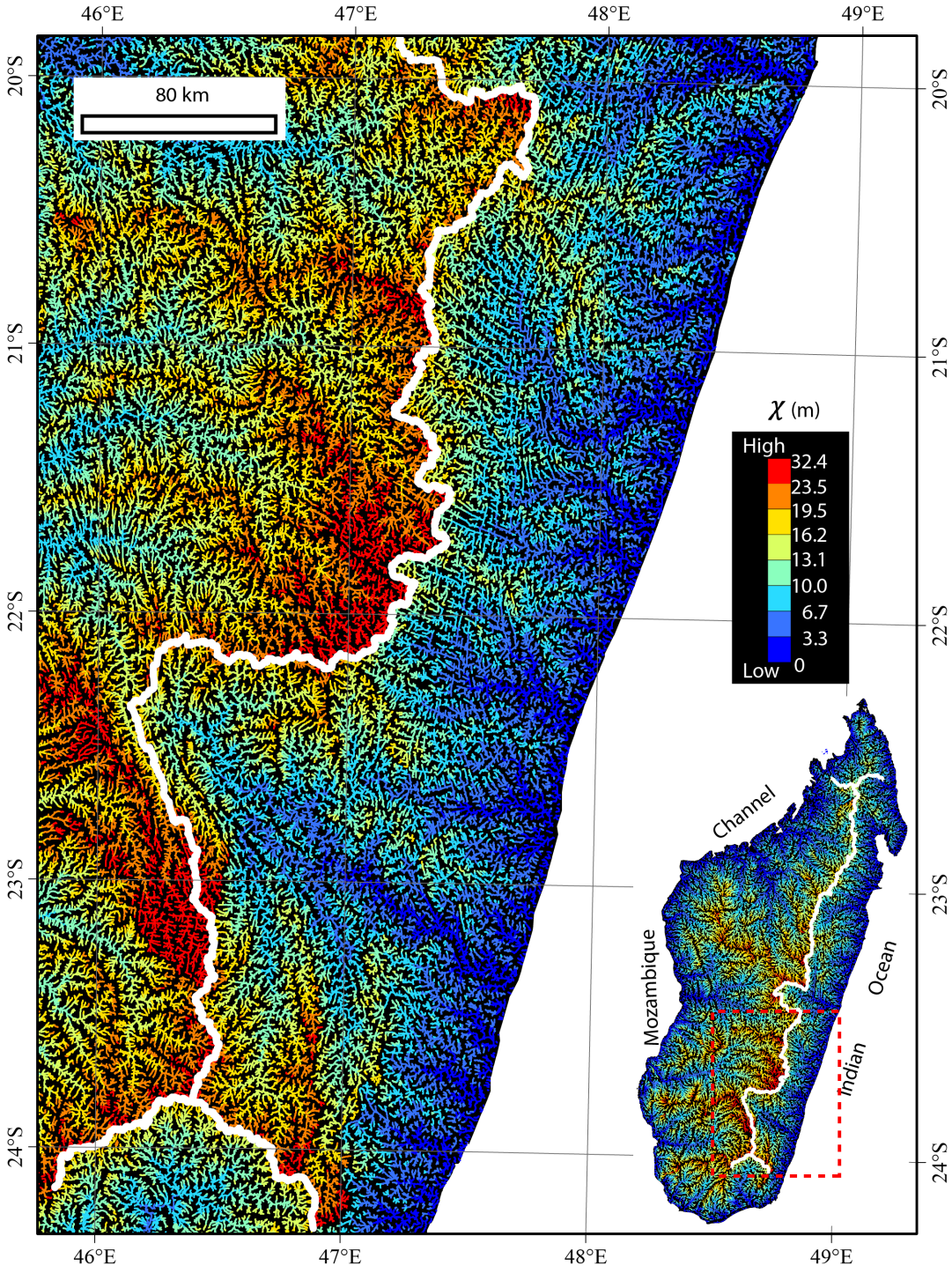

Figure 4. Systematic χ (m) contrast of channel heads across the major water divide (the thick white line): high χ on west side and low χ on east side of the major divide. χ calculation follows Perron and Royden (2013) and includes the mean annual precipitation. χ calculation uses reference drainage of 1 km^2, reference annual precipitation of 1000 mm/year, concavity of 0.45 and base level of sea level.

Escarpment-draining rivers of Madagascar display two distinctive morphologies (Figure 5). From the outlet to the water divide, a coastal plain river abruptly steepens at the escarpment foot, then flattens again at the top of the escarpment (Type B on Figure 5).

Alternatively, many escarpment rivers have no upper low-steepness reach. Instead, these retain high steepness until their divide at the top of the escarpment (Type A on Figure 5). Both types of escarpment river are segmented in the same way on the transformed χ-elevation profile.

The two distinctive types of escarpment rivers co-exist even within a single catchment. In the Namorona River basin, for example, 78% of the major escarpment rivers are Type B and 22% are Type A (Figure 6a-c). The escarpment edge is shown as a triangle on Figure 6a-c. The escarpment edge appears as a slope-break point on the Type B rivers. The conventional view of a suite of knickpoints within a single catchment is that they are a consequence of a common, temporal change of uplift. This is testable, either by the common elevation to these knickpoints or by plotting the χ profiles of all rivers and checking that they collapse onto one common profile with co-located knickpoints. The Madagascar escarpment rivers do not exhibit common morphologies. The elevation of the knickpoints varies by 500 meters and they occur over a wide range of χ values (Figure 6d). Although spatial variations in rock uplift rate or in erodibility can lead to variance in χ or elevation, uplift rates in a tectonically inactive area will not vary significantly over the short wavelength of a single catchment and there are no major lithologic changes within most catchments. Furthermore, there is no systematic spatial pattern to the knickpoint χ values within a single catchment or between catchments. The co-existence of Type A and Type B rivers within a single catchment and the high variance in the escarpment edge χ and elevation are common across Madagascar (Supplement Figure S1-S5), and suggests that it is local, not regional (common uplift) processes dictating the morphology of the river profiles.

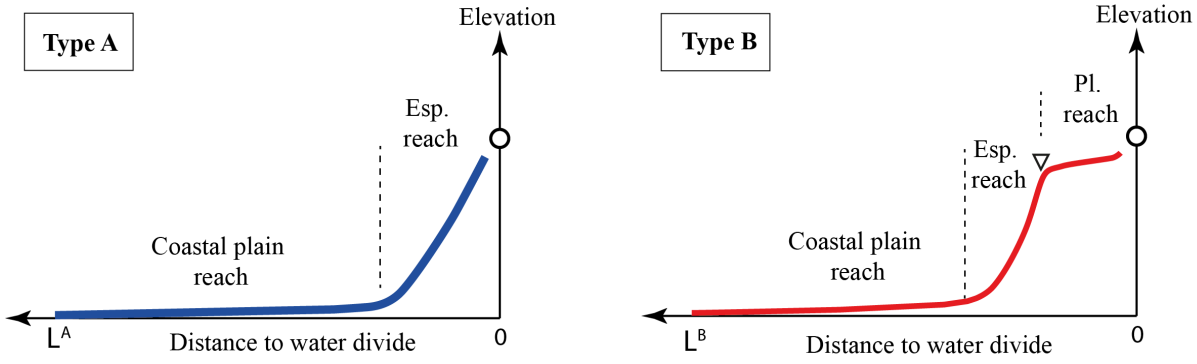

Figure 5. Illustration of two distinctive types of river profiles in Madagascar escarpment. The circle is the water divide. The triangle indicates the escarpment edge, where this is identifiable as a knickzone. Pl. and Esp. are short for plateau and escarpment respectively.

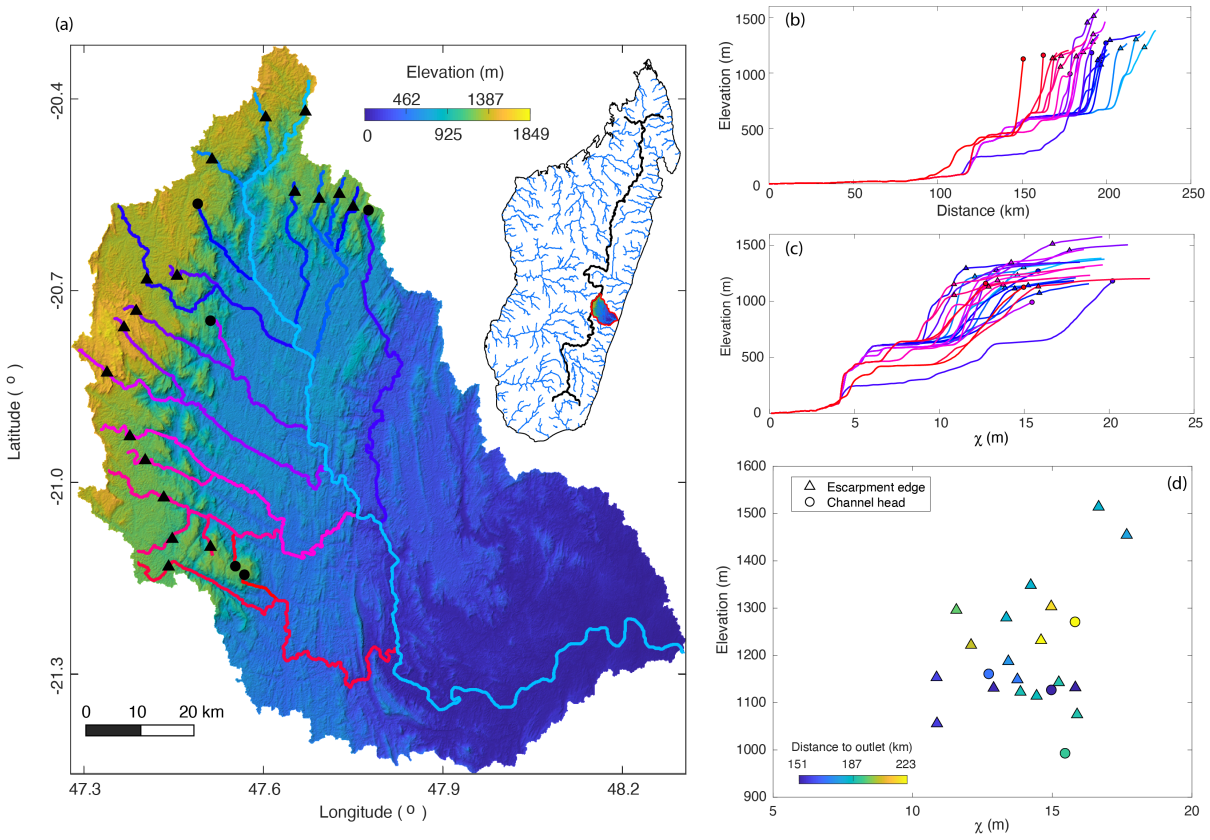

Figure 6. (a) SRTM digital elevation model (Jarvis et al., 2008) of an escarpment-draining basin, the Namorona River basin in Madagascar. Basin location is indicated in the inset. Rivers are extracted from DEM with threshold channel head area of 1 km^2. (b) river profiles (c) transformed χ-elevation profile. (d) Position of the escarpment edge at a channel and χ value of the escarpment edge where this is identifiable as a knickzone or the channel head where there is no knickzone.

3 Methodology of interpreting DCN ^{10}Be concentration

An important means of determining landscape evolution patterns and rates is by establishing rates of surface change. In this study, we present new detrital cosmogenic nuclide (DCN) (^{10}Be) concentrations to calculate conventional erosion rates as well as applying the recently proposed method for determining escarpment retreat rates directly from these data (Wang and Willett, 2021).

3.1 Sampling strategy and analytical procedures for river sediments

We measured catchment-wide erosion rates with *in-situ* produced cosmogenic ^{10}Be concentrations from 29 river sand samples. River sand samples were collected from active channels in drainage basins on both sides of the continental water divide and cover most of the escarpment area (Figure 1). According to the geomorphic features, we divide ^{10}Be basins into three types of catchments (Figure 1). If the outlet is within the central plateau, the basin is a plateau basin. If rivers in a basin are fully on the lowland, it is a coastal plain basin. Rivers that include the steep escarpment reach and parts of either the plateau or the coastal plain are referred to as escarpment rivers. Escarpment rivers can be either type A or B.

Escarpment and coastal plain basins are in the tropical rainforest area and are less likely to be affected by anthropogenic processes. Plateau basins close to the city of Antananarivo were sampled upstream of the city (Sample 24 and 25 on Figure 1). Sampled basins are between 16 and 17478 km^2 in area.

To help assure that samples are representative of the whole catchment, river sediment from active channels were amalgamated from samples collected for 200-500 meter along the channel. Sediments were sieved into different grain size fractions. Grain size fraction 250-500 μm and 125-250 μm was used for quartz purification. Quartz was purified from sieved sediments following methods of Lupker et al. (2012): magnetic separation, dissolution in mixed H_2SiF_6 and HCl, then three to five rounds of HF of etchings to remove meteoric Be. Be was purified following established protocols by Ochs (1996). Purified quartz was dissolved with HF together with ~0.3 mg of a commercial carrier solution (Scharlau). Be was purified by removal of other elements through cation and anion chromatography. BeOH was precipitated and transformed into BeO at 1000°C. Targets for accelerator mass spectrometry (AMS) measurements were prepared and $^{10}Be/^{9}Be$ ratios were measured at the ETH Zurich Tandy facility (Christl et al., 2013). The measured $^{10}Be/^{9}Be$ ratio was normalized to the S2007N standard with a nominal $^{10}Be/^{9}Be$ ratio of 28.1 (±0.76) × 10^{-12} (Christl et al., 2013) which is in accordance with ^{10}Be half-life $t_{1/2}$ of 1.387 (±0.012) × 10^6 years (Chmeleff et al., 2010). An average $^{10}Be/^{9}Be$ blank ratio of 8.1 (±0.70) × 10^{-15} was subtracted from the measurements. Uncertainty of blank corrections were also used to correct the uncertainty of measurements. After corrections of blank and blank uncertainties, the $^{10}Be/^{9}Be$ ratio of each measurement was converted to ^{10}Be concentration in atoms per gram of quartz. These concentration data are directly used in calculations of erosional mass flux.

3.2 Mass flux calculation

Wang and Willett (2021) proposed a method for analysis of detrital cosmogenic nuclide concentrations in terms of a directional mass flux. Assuming secular equilibrium of cosmogenic nuclide production and export, the measured detrital cosmogenic nuclide concentration can be regarded as a ratio between nuclide production and dilution into a sediment volume. The volume of sediment is defined by the flux of rock through the Earth's surface, but this flux needs not be vertical. Here we use this analysis method to calculate both the conventional erosion rate (i.e. vertical mass flux) and the escarpment retreat rate (i.e. horizontal mass flux) from ^{10}Be concentrations. As a general expression,

$$\left|\overrightarrow{F_s}\right| A_{eff} = \frac{\iint_S \Lambda P_0(x,y)\,dx\,dy}{\rho C} \tag{1}$$

Where the $\left|\overrightarrow{F_s}\right|$ is the magnitude of the mass flux vector $\overrightarrow{F_s}$. A_{eff} is the effective area of the catchment surface projected onto a plane normal to the direction of the mass flux: if the mass flux $\overrightarrow{F_s}$ is vertical, the effective area A_{eff} is the basin area as conventionally calculated, for example from a DEM; if $\overrightarrow{F_s}$ is horizontal, a projected area for the basin surface onto a vertical plane is used in Equation (1). ρ (gram/cm^3) is the density of the target, Λ (gram/cm^2) is the free path absorption length, $P_0(x,y)$ (atoms $gram^{-1}year^{-1}$) is the production rate of the cosmogenic nuclide at the surface at any given geographic location (x,y), S is the basin surface, and C (atoms/gram) is the measured concentration of in-situ cosmogenic nuclides. A

continuous catchment surface S can be approximated by discretized elemental surfaces from a digital elevation model (DEM). The calculation of the surface integral in Equation (1) is approximated by the summation of discretized elemental surfaces k of the catchment surface:

$$\iint_S \Lambda P_0(x,y)\,dxdy = \sum_k \Lambda P_0^k \Delta x \Delta y \quad (2)$$

where P_0^k is the production rate of cosmogenic nuclides at the surface for a given elemental surface k. *In situ* cosmogenic ^{10}Be has three production pathways: neutrons, slow muons and fast muons. In practice, the production nuclides from the three pathways are summed together to represent the overall cosmogenic production P_0^k (Lupker et al., 2012):

$$\Lambda P_0^k = \sum_i \Lambda_i P_{0i}^k \quad (3)$$

where Λ_i and P_{0i}^k are the free path absorption length and surface production rate of the pathway neutrons, slow muons and fast muons respectively.

Equations (1) to (3) are built on the assumption that radioactive decay can be neglected, which should be true as long as the condition $\left|\overrightarrow{F_s}\right|\rho/\Lambda_i \gg \lambda$ is met (von Blanckenburg, 2006) where $\lambda = ln2/t_{1/2} \approx 1.38 \times 10^{-6} yr^{-1}$ for 10Be (Chmeleff et al., 2010). The effective attenuation length of neutrons, slow muons and fast muons of ^{10}Be is 160, 1500 and 4320 gram/cm^2 respectively (Braucher et al., 2011). To calculate the surface production rates P_{0i}^k of different pathways, the 10Be production rate due to neutrons, slow muons and fast muons were scaled for latitude and local altitude (Stone, 2000). The sea level high latitude (SLHL) production rate of 3.97(±0.1) atoms/gram/yr (Balco et al., 2008) is used, following the methodology of Lupker et al. (2012). We did not apply any topographic shielding correction (DiBiase, 2018).

3.3 Partition of the erosional mass flux across geomorphic zones

Although the continental water divide closely parallels the escarpment edge in Madagascar, it coincides with the escarpment edge only about 32% of the time (Figure 1). It is unclear if this morphology represents the steady form of the escarpment which is retreating while maintaining that form, or if the plateau reach represents a transient feature, for example as the remnant of a recent river capture event. If the former is true, the horizontal flux calculation would be correct, but if the latter is the case, it is possible that the plateau is downcutting in a transient mode that could affect ^{10}Be concentrations. If the divide is far from the escarpment, e.g. basin 13 in Figure 1, the erosional mass flux of this escarpment-draining basin could come from both the downcutting of the plateau and the backcutting of the escarpment. We can partition the flux between the two as a correction to the purely horizontal retreat rate. We assume that a catchment has a high plateau area A_p with an erosion rate of e_p and that the escarpment is characterized by a mass flux rate of v through a vertical plane with area, A_r. The overall mass from measured DCN ^{10}Be concentration C in Equation (1) is a partition of mass between the plateau erosion and the escarpment retreat:

$$e_p A_p + v A_r = \frac{\iint_S \Lambda P_0(x,y)\,dx\,dy}{\rho C} \quad (4)$$

In order to use Equation (4) to correct for the retreat rate v, the plateau erosion rate e_p must be constrained independently, which we do by using the mean erosion rate of plateau basins.

3.4 Correction for flexural uplift on ^{10}Be-inferred retreat rates

Isostatic uplift from erosion of the escarpment creates a vertical velocity which, if eroded, must also be accounted for in the basin-wide erosional mass. If this isostatic uplift is distributed by lithospheric flexure, it will lead to uplift of both the plateau and the coastal plain below the escarpment. Uplift of the plateau has no effect on our calculations, but uplift of the coastal plain, and the escarpment will affect the mass flux estimate. Assuming that all flexural uplift is removed by erosion, the ratio of isostatically-uplifted mass removed relative to the retreat mass removal (R_A) depends on the lithospheric rigidity and the flexural wavelength and can be expressed as (Wang and Willett, 2021):

$$R_A = \frac{\rho_{crust}}{2\rho_{mantle}} * \left(\exp\left(-\frac{X_c}{\alpha}\right)\cos\left(\frac{X_c}{\alpha}\right) - 1\right) \quad (5)$$

In this expression, X_c is the distance between the midpoint of the escarpment and the ^{10}Be sampling location. Density of the mantle and the crust is given by ρ_{mantle} and ρ_{crust} respectively. α is the wavelength of isostatic deflection (Turcotte and Schubert, 2002). Equation (5) gives the vertical isostatic component of the mass flux as a correction to the inferred retreat rate and will be presented with the main results.

4 Erosion rates of Madagascar: central plateau and east margin

4.1 Erosion rates of Madagascar

We calculated erosion rates from measurement of 29 DCN ^{10}Be concentrations. DCN ^{10}Be concentrations from Cox et al. (2009) are also included, but recalculated according to a common protocol. Basins in our area can be divided into two groups: the active graben-related basins and the escarpment-related basins, which are further subdivided as discussed above in terms of morphology. The highest erosion rates in our study area are found in basins affected by graben extension. Erosion rates of the graben-related basins are between 23.1-34.3 m/Ma. For the escarpment system, the north-south trending continental water divide and the escarpment define four geomorphic zones: the plateau west of the divide, the plateau east of the divide, the escarpment, and the lowland plain (Table 1). Erosion rates are generally lower on the plateau and on the coastal plain, and are higher if the catchment includes the escarpment (Figure 7, Table 1). Erosion rates for plateau basins are between 5.8-12.1 m/Ma. Plateau basins (8, 18, 19 and 22) are eroding at similar rates, falling in a narrow range of 7.4-10.3 m/Ma. Erosion rates for escarpment basins within Lat. 20° S - 22° S are between 13.1-26.0 m/Ma. Escarpment basins in the far south (south of Lat. 22° S) have lower erosion rates

of 8.7-14.2 m/Ma. The one basin entirely on the coastal plain has an erosion rate of 6.4 m/Ma.

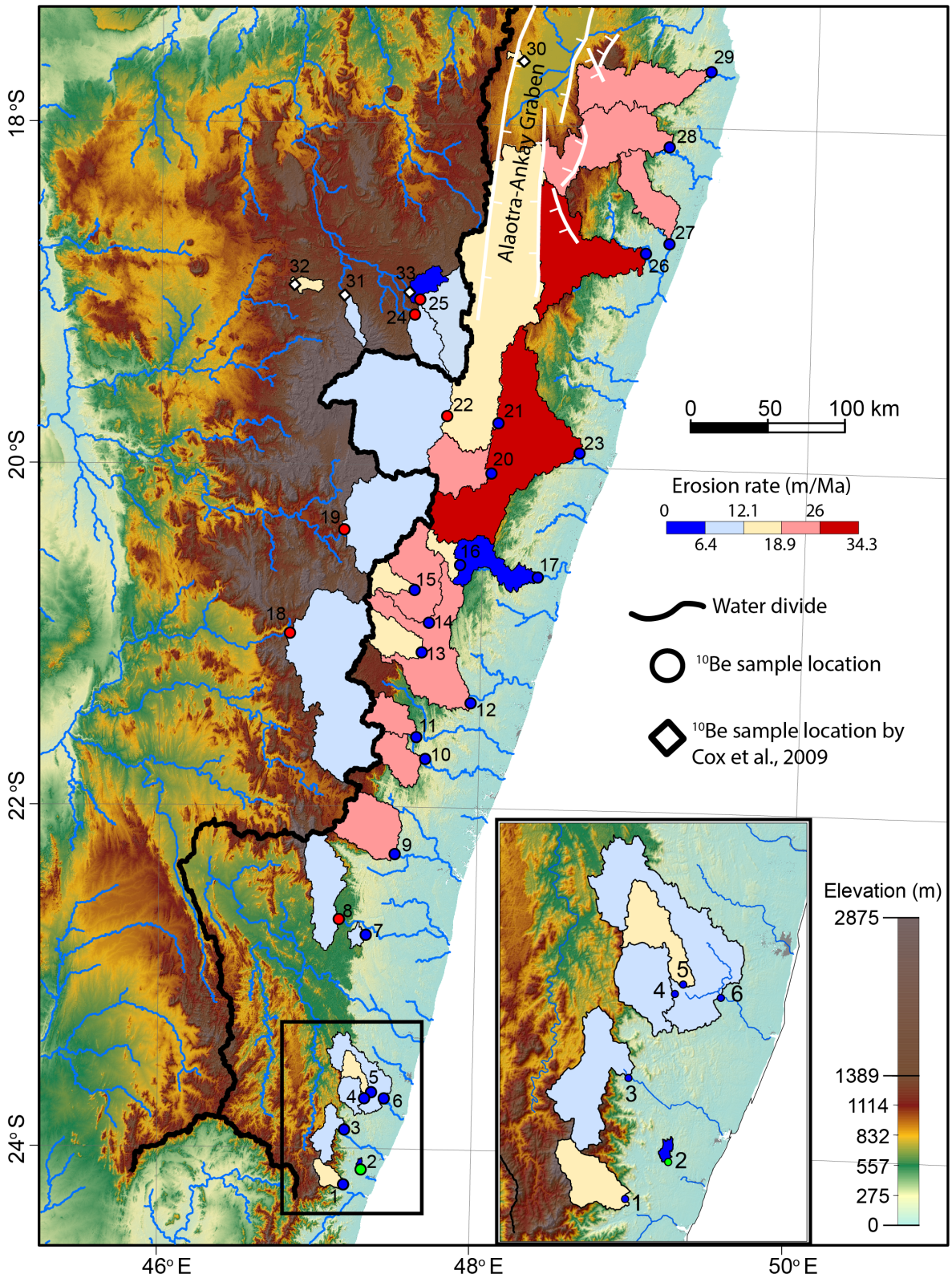

Figure 7. Erosion rates of Madagascar from detrital cosmogenic ^{10}Be concentrations. Erosion rates are lower west of the continental water divide, for basins entirely on the plateau, or

entirely on the eastern coastal plain. Higher rates are found for the escarpment-draining catchments and for those associated with the Alaotra-Ankay graben.

Table 1. Summary of ^{10}Be sample locations, concentrations and erosion rates of Madagascar

Source	Basin	Basin number	Lon. (°)	Lat. (°)	^{10}Be concentration ±1σ ($\times10^3$ atoms g^{-1})		Erosion (m/Ma) [b]			Basin Area (km^2)	Surface production rate[c] (atoms g^{-1} yr^{-1})		
							Rate	-34%	+34%		*Pn*	*Pms*	*Pmf*
Great escarpment system: escarpment basins													
This study	MDG_1653D2	1	47.1890	-24.2261	334.2	13.9	14.2	1.72	1.68	209	6.316	0.018	0.048
This study	MDG_1631B1	3	47.1941	-23.9125	462.6	16.1	10.2	1.21	1.19	407	6.259	0.018	0.048
This study	MDG_1609A1	4	47.3113	-23.7058	281.5	10.0	10.3	1.45	1.42	274	3.549	0.013	0.041
This study	MDG_1586D1	5	47.3339	-23.6822	240.7	7.8	12.9	1.69	1.79	231	3.845	0.014	0.042
This study	MDG_1610A1	6	47.4275	-23.7135	340.6	11.5	8.7	1.20	1.18	1225	3.616	0.013	0.041
This study	MDG_1460C1	7	47.3134	-22.7545	282.5	11.1	10.9	1.50	1.50	108	3.770	0.014	0.042
This study	MDG_1405A1	9	47.4951	-22.2744	144.8	7.7	24.1	3.17	3.41	1262	4.434	0.015	0.044
This study	MDG_1318A2	10	47.6524	-21.7258	136.9	5.7	26.0	3.44	3.42	656	4.512	0.016	0.045
This study	MDG_1287B2	11	47.5869	-21.5768	155.6	8.2	26.0	3.42	3.36	517	5.281	0.017	0.047
This study	MDG_1234D1	12	47.9314	-21.3138	157.8	8.9	25.4	3.21	3.43	4992	5.197	0.017	0.047
This study	MDG_1204C1	13	47.6379	-21.1063	286.2	12.8	16.0	2.00	1.96	690	6.032	0.019	0.049
This study	MDG_1176C1	14	47.6687	-20.9162	201.9	11.3	22.7	2.89	2.92	1863	6.027	0.019	0.049
This study	MDG_1147D1	15	47.5790	-20.7290	294.2	8.1	18.1	2.04	2.01	377	7.143	0.021	0.052
This study	MDG_1122C1	16	47.8701	-20.5835	290.5	11.7	15.7	1.92	1.91	290	5.954	0.019	0.049
This study	MDG1152B1[a]	17	48.3419	-20.6250	959.2	32.8	3.8	0.5	0.5	1189	5.954	0.019	0.049
This study	MDG_1038C1	20	48.0539	-20.0409	224.5	14.7	20.8	2.64	2.84	1091	6.215	0.019	0.049
Great escarpment system: coastal plain basin													
This study	MDG_1654A2	2	47.2928	-24.1229	402.9	12.0	6.4	0.90	0.94	16	3.090	0.012	0.040
Great escarpment system: plateau basins													
This study	MDG_1011B1[a]	22	47.7657	-19.7108	896.8	43.5	7.4	0.87	0.84	4380	7.504	0.020	0.045
This study	MDG_1089D1	19	47.1334	-20.3778	596.5	24.6	10.2	1.17	1.17	2638	8.326	0.023	0.054
This study	MDG_1459B1	8	47.1262	-22.6196	399.4	13.3	10.3	1.25	1.26	1272	5.378	0.017	0.047
This study	MDG_1199B1	18	46.8104	-20.9848	600.7	21.3	8.8	1.03	1.01	4762	7.160	0.021	0.051
this study	MDG_Antana2	24	47.5681	-19.0939	607.3	17.5	9.7	1.09	1.07	626	8.066	0.023	0.054
this study	MDG_Antana1	25	47.5942	-19.0228	488.6	15.1	12.1	1.35	1.33	1257	8.034	0.023	0.054
Cox et al., 2009	Cox_2004-6A[a]	31	47.1251	-19.0045	590.0	18.0	9.7	1.1	1.1	209	8.053	0.023	0.054
Cox et al., 2009	Cox_2004-2A	32	46.8227	-18.9452	370.0	14.0	14.5	1.7	1.7	134	7.260	0.021	0.052
Cox et al., 2009	Cox_2004-9A	33	47.5259	-18.9500	1000.0	23.0	5.8	0.7	0.6	1541	7.977	0.022	0.054
Alaotra-Ankay Graben-related basins													
this study	MDG_1013B1	21	48.0801	-19.7531	288.9	15.4	18.8	2.33	2.33	11508	7.335	0.021	0.052
this study	MDG_1042A1	23	48.5896	-19.9178	141.8	8.6	34.3	4.33	4.45	17478	6.462	0.020	0.050
this study	MDG_0848C1	26	48.9739	-18.7315	113.4	5.5	33.9	4.38	4.43	2624	4.904	0.017	0.046
this study	MDG_0849A2	27	49.1057	-18.6831	132.8	8.6	23.1	3.35	3.48	1051	3.769	0.015	0.043
this study	MDG_0754A2	28	49.1051	-18.1115	157.9	6.7	25.3	3.34	3.05	1679	5.426	0.018	0.048
this study	MDG_0657C1	29	49.3400	-17.6602	153.4	6.5	24.4	3.28	3.19	1936	4.753	0.017	0.046
Cox et al., 2009	Cox_2005-7	30	48.2041	-17.6280	210.0	6.0	18.9	2.3	2.3	56	5.128	0.018	0.048

(a) Basaltic surface area is excluded from ^{10}Be production calculation.
(b) The conventional erosion rate is calculated from Equation (1). ^{10}Be concentrations from Cox et al. (2009) are recalculated for consistency.
(c) Mean basin ^{10}Be production rates of neutrons (*Pn*), slow muons (*Pms*) and fast muons (*Pmf*). Calculation method follows Lupker et al. (2012).

4.2 Retreat rates of the Madagascar escarpment

Horizontal retreat rates for the escarpment are calculated from the ^{10}Be concentrations as in Wang and Willett (2021). Calculation of a horizontal retreat rate requires selection of a direction. We took a constant direction of N73W, as normal to the coastline and the offshore continental shelf margin. This direction is used to calculate the projected area A_r of the escarpment basin surface. The escarpment is not perfectly parallel to the coast, particularly where it is influenced by the active Alaotra-Ankay Graben north of Lat. 20° S. South of 20° S, the escarpment segment is morphologically more uniform, so we have focussed our study here. Retreat rates are between 182-1886 m/Ma (Figure 8a, Table 2). The escarpment segment that is bounded by escarpment basins 1-7 is retreating slowly at rates of 182-548 m/Ma. The northern segment that is bounded by escarpment basins 9-20 is retreating faster, at rates of 448-1886 m/Ma. Variations in retreat rates correspond to the distance of the escarpment to the coastline (Figure 8a), suggesting that the current variations in retreat rate are representative of the rates over the post-rift time period.

As most of our escarpment-draining basins have a significant plateau area, we calculated a corrected retreat rate accounting for downward erosion of the plateau area. For this correction, we use the erosion rate measured for the four basins that exclusively drain from the plateau and have few hillslope collapse features (lavakas) (Plateau Basins 22, 19, 8 and 18 on Figure 1). The average erosion rate for these basins is 9.17 m/Ma. Corrections for plateau area are mostly within the range of ±10% (Table 2).

We also applied the correction for the flexural uplift of the coastal plain and escarpment. We calculated corrected retreat rates for different lithospheric rigidities (Supplement Table S1). For Table (3) we use a value of 20 km for the effective elastic thickness of the lithosphere. These corrections are always downward, and are up to several tens of percent of the estimated retreat rate. Corrections are mostly less than 25% (Table 3).

Retreat rates after corrections for both plateau area and flexural uplift of the coastal plain are smaller than the non-corrected retreat rates but maintain the pattern of spatial variability (Figure 8b).

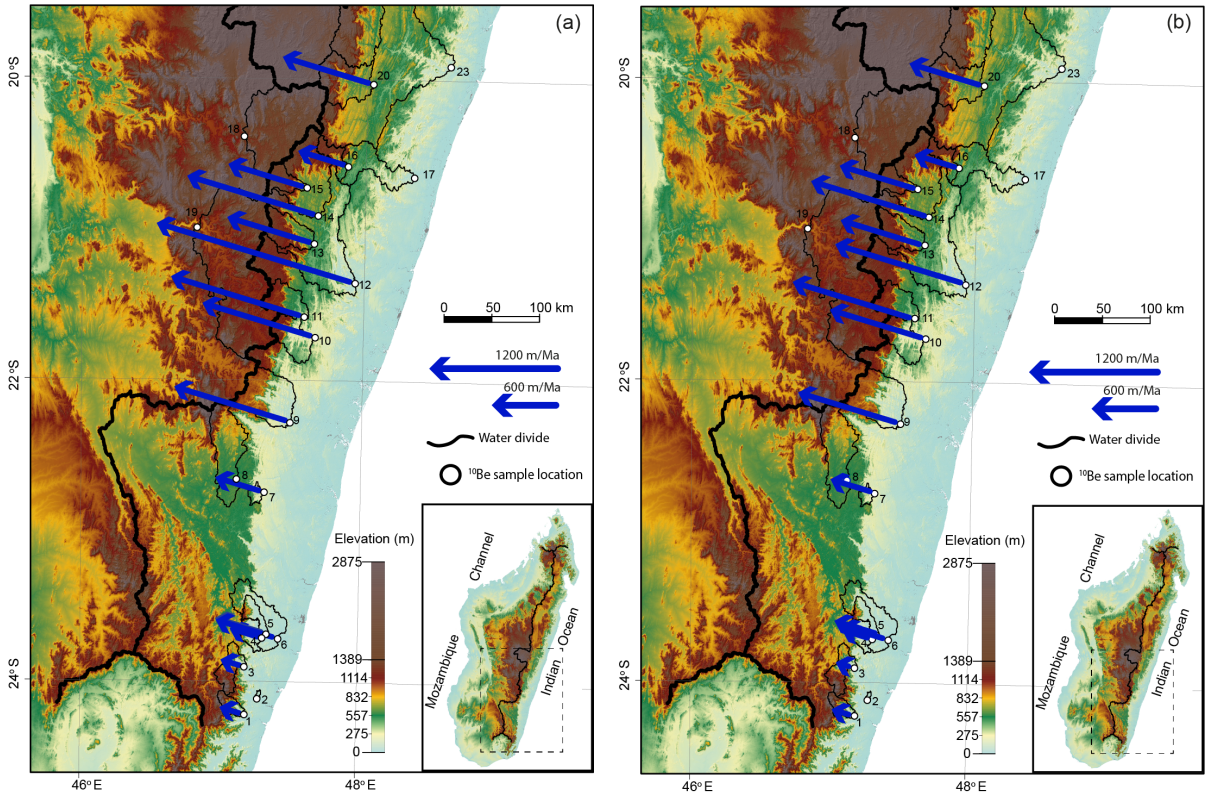

Figure 8. Escarpment retreat rates calculated from detrital cosmogenic ^{10}Be concentrations (a) with no correction (b) corrected for plateau area and flexural rebound (T_e = 20 km). Arrows represent retreat vectors. The direction is fixed at N73W; vector length represents retreat rate (see Table 2 and Table 3 for the data).

436 **Table 2**. Escarpment retreat rates for basins of Madagascar

Basin	Distance[a] (km)	Retreat rate (m/Ma) no correction			Plateau area (km^2)	ESP_k_{sn} [c] ($m^{0.9}$)	Basin_k_{sn} [b] ($m^{0.9}$)	Retreat rate (m/Ma) corrected for plateau area [d]			Correction (%)	Basin number
		Rate	-34%	34%				Rate	-34%	34%		
MDG_1653D2	35.6	188.7	22.8	22.2	25	169	142	181.1	23.9	23.9	-4	1
MDG_1631B1	45.1	181.8	21.6	21.2	267	166	97	131.9	31.8	31.3	-27	3
MDG_1609A1	46.1	267.5	37.5	36.7	0	101	33	No need of a correction				4
MDG_1586D1	45	447.6	58.8	62.1	37	158	57	463	64.5	63.3	3	5
MDG_1610A1	45.5	548.3	75.8	74.8	268	121	34	515.6	80.2	76.6	-6	6
MDG_1460C1	63	425.1	58.4	58.4	20	64	27	411.8	57	60.7	-3	7
MDG_1405A1	72.9	1083	142.3	153.2	445	132	51	1176.5	172.4	183.8	9	9
MDG_1318A2	76.6	1051	139.3	138.3	146	131	54	1062.6	147.5	145.1	1	10
MDG_1287B2	85.5	1247.7	164.3	160.6	235	125	50	1353.5	198.8	202.3	8	11
MDG_1204C1	96.5	802.3	100.5	98.2	367	120	53	896.8	142.6	145.2	12	13
MDG_1147D1	105	718.1	81	79.6	266	142	48	767.7	130.4	121.6	7	15
MDG_1176C1	101.3	1228.6	156.7	158	709	119	47	1351	187.8	202	10	14
MDG_1234D1	99.2	1886	238.5	254.4	1144	111	49	2037.6	282.4	294.5	8	12
MDG_1038C1	96.1	838.2	106.2	114.2	418	121	62	850.6	119.8	118.2	1	20
MDG_1122C1	81.4	441.1	52.6	54.5	153	150	62	416.4	68	67.1	-6	16

437 (a) Distance of the basin-bounded escarpment segment to the coastline. Distance is calculated
438 using a reference retreat direction of N73W.
439 (b) Mean river steepness (k_{sn}) of the basin. k_{sn} is calculated from the integral method
440 (topographic gradient in χ space (Perron and Royden, 2013)) with precipitation included, m/n
441 of 0.45 for rivers with threshold drainage 1km^2.
442 (c) Mean river steepness (k_{sn}) of the escarpment reach. A threshold of k_{sn}=35 is used to filter
443 out upper plateau reach and low land reach.
444 (d) Correction method follows Equation (4). Madagascar basins are corrected by an average
445 plateau erosion rate of 9.17 m/Ma.

446

447 **Table 3**. Flexural rebound correction for escarpment retreat rates for basins of Madagascar.

Basin	[a]R_A (%) ([b]Te = 20km)	Retreat rate (m/Ma) Corrected for flexural only (Te = 20 km)			Corrected for both flexure (Te = 20 km) and plateau area				Basin number
		Rate	-34%	+34%	Rate	-34%	+34%	[c]Correction impact (%)	
MDG_1653D2	8.4	173	21	20	166	22	22	-12	1
MDG_1631B1	7.6	168	20	20	122	29	29	-33	3
MDG_1609A1	10.6	239	33	33	239	34	33	-11	4
MDG_1586D1	15.2	380	50	53	393	55	54	-12	5
MDG_1610A1	22.0	428	59	58	402	63	60	-27	6
MDG_1460C1	6.4	398	55	55	385	53	57	-9	7
MDG_1405A1	19.6	871	114	123	946	139	148	-13	9
MDG_1318A2	16.7	875	116	115	885	123	121	-16	10
MDG_1287B2	16.0	1048	138	135	1137	167	170	-9	11
MDG_1204C1	14.8	684	86	84	764	121	124	-5	13
MDG_1147D1	7.1	667	75	74	713	121	113	-1	15
MDG_1176C1	18.2	1005	128	129	1105	154	165	-10	14
MDG_1234D1	40.1	1130	143	152	1221	169	176	-35	12
MDG_1038C1	20.6	666	84	91	675	95	94	-19	20
MDG_1122C1	7.1	410	49	51	387	63	62	-12	16

448 (a) The ratio of isostatically-uplifted mass removed relative to the retreat mass removal in Equation
449 (5) for a density ratio of 0.85 between the crust and the mantle.
450 (b) Effective elastic thickness of the lithosphere.
451 (c) Compared to the uncorrected retreat rates in Table 2.
452

453 ## 5 Discussion

454 ### 5.1 Morphology and rates of landscape change

455 Erosion rates across Madagascar vary systematically with morphology. Our basins
456 confined to the plateau have an average erosion rate of 9.7 m/Ma, which is similar to other
457 plateau basins inland of a great escarpment, e.g. the Serra do Mar in southern Brazil (9.2

m/Ma) (Salgado et al., 2016), the Deccan Plateau inland of the Western Ghats escarpment of India (9.6 m/Ma) (Mandal et al., 2015). The average erosion rate for the escarpment basins of Madagascar is higher, but still low at 16.6 m/Ma. It is among the lowest rates measured for passive margin escarpments, compared for example to the Western Ghats escarpment (48.6 m/Ma) (Mandal et al., 2015), the southeastern Australian escarpment (32 m/Ma) (Godard et al., 2019) , the southeastern Brazil escarpment (30.2 m/Ma) (Salgado et al., 2016). However, this rate does not reflect the erosion rate of the steep escarpment as there are no basins restricted to the escarpment. Most escarpment basins in our study have a significant portion of flat plateau. The plateau area represents 12% to 71% of escarpment-draining basins (Table 2). Although difficult to isolate, erosion rates of escarpment basins are substantially higher than the inland plateau basins, implying differences in erosional processes and efficiency.

Plateau basins are characterized by gentle slopes and deeply weathered saprolite, implying a lack of fluvial incision even though the precipitation rate is often high. The high precipitation rate of plateau basins facilitates *in situ* weathering, instead of providing fluvial incision power, given the low channel slopes. Erosion of the plateau might be limited by weathering, rather than physical erosion.

For their erosion rate, the escarpment basins of Madagascar have some of the highest river steepness indices measured worldwide (Figure 9). In contrast, the plateau basins, the coastal plain basin and basins related to the active graben are consistent with more typical values of river steepness and observed erosion rate. The very high river steepness of Madagascar escarpment rivers relative to the global empirical relationship of river steepness and erosion rate supports the model of concentrated erosion at the escarpment and supports the model of horizontal retreat (Willett et al., 2018).

Interpreted as horizontal retreat rates instead of vertical erosion rates gives a very different view of the landscape dynamics. Escarpment rivers are driving escarpment retreat at rates of up to 1200 m/Ma (Figure 8). These high rates of retreat explain the steepness of the escarpment reaches as well as the structure of the river profiles with steep escarpments contrasting with flat coastal plains and plateaus. Retreat of the water divide into the plateau and the subsequent, but sporadic, river capture explains the large number of segmented river profiles and the variability between profiles within single basins. Landscape evolution dominated by erosion focused onto the escarpment thus provides an explanation for the morphological observations and the high concentrations of ^{10}Be, reconciling these seemingly contradictory observations.

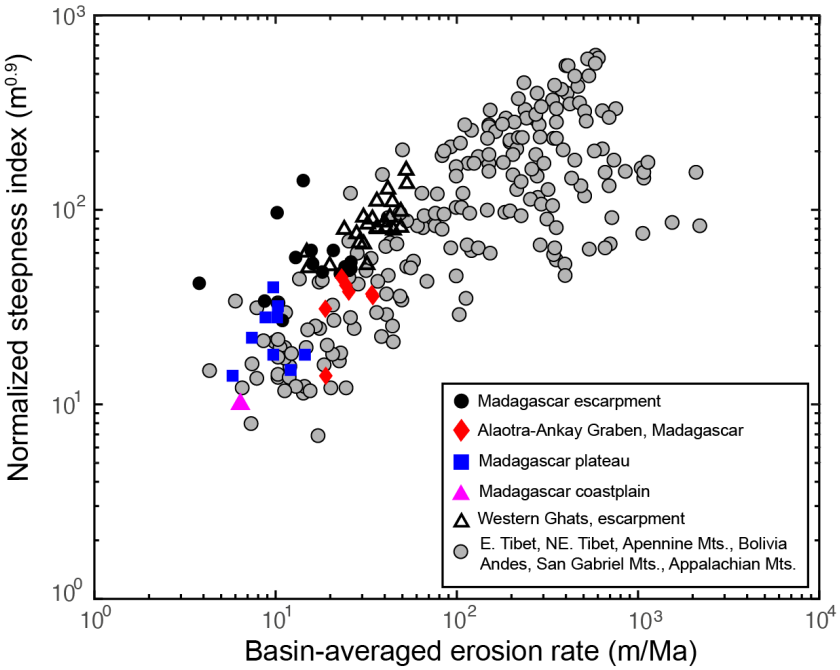

Figure 9. Normalized channel steepness index and cosmogenic ^{10}Be-derived basin-averaged erosion rate of Madagascar, with comparison to a compilation of global data by Kirby and Whipple (2012) (grey colored dots) and Southern Western Ghats (black-lined triangles).

The basins in the active Alaotra-Ankay Graben display some of the highest vertical erosion rates of our study area and are likely to be characterized by vertical erosion. Apart from one basin from Cox et al., 2009, which is located on the margin of the Alaotra lake (basin 30 on Figure 1), the other basins of this group also comprise a prominent relief zone, similar to the regional escarpment (Figure 1). The average erosion rate of the graben basins is 27 m/Ma, higher than the great escarpment basins although the graben basins are characterized by gentler slopes and variable precipitation rates.

Active faulting of the graben, coincident with the high rainfall in this area, probably triggered the widespread hillslope failure. Intensive, localized hillslope erosion along the footwalls of normal faults occurs through gully erosion (Kusky et al., 2010; Voarintsoa et al., 2012), a phenomenon that results in formation of geomorphic features referred to as "lavakas" in Madagascar (Figure 10). These lavakas develop on thick laterite-saprolite mantled hillslopes (Wells et al., 1997; Wells and Andriamihaja, 1990). The collapse of hillslopes excavates deeply into the saprolite, exporting a significant amount of highly weathered sediment into the rivers. The deep erosion of the hillslope failure in the lavakas results in a lower cosmogenic ^{10}Be concentration compared with normal hillslope colluvium sediment (Cox et al., 2009). In places, tens of lavakas can be found per square kilometer (Cox et al., 2010). The graben basins in our study area are fed with lavaka sediment and this could contribute to the higher erosion rates measured from cosmogenic ^{10}Be concentrations.

Figure 10. Erosional feature known as a lavaka in Madagascar. Location of the photo is indicated in Figure 1.

5.2 Comparison between the conjugate margins of Madagascar and India

Retreat rates and morphology of the margins of Madagascar and India are compared in Figure 11. Lithological differences between the two conjugate margins are likely minimal, as both developed on the Precambrian shield and the surface geology is primarily metamorphic rock of the shield. The precipitation rate of the Western Ghats escarpment is generally larger than the Madagascar escarpment, but is dominated by heavy seasonal monsoon rains. Erosion rates of the escarpment-draining basins from Western Ghats are higher than the Madagascar escarpment-draining basins (Figure 9). After correction for plateau area and flexural compensation, the retreat rates of Western Ghats, however, are similar to the Madagascar escarpment (Figure 12). Both margins show the same correlation of modern rate with escarpment distance from the coastline.

The retreat rates we obtain are close to the average retreat rate since rifting (Figure 12), although our rates are systematically lower, suggesting that rates were faster shortly after rifting, or that the timescale of ^{10}Be accumulation is not capturing the Ma-average properly. The discrepancy is also dependent on the age which we take for the onset of escarpment retreat. Some constraints are provided for the age of rifting in Figure 12, but escarpment retreat would have initiated very early in the rifting process. Once continental rift structures were established and rivers were diverted, a mobile divide would form and begin migration. We expect that this would have occurred as early as 120 Ma and certainly before 100 Ma, so the difference between long-term and ^{10}Be-based retreat rates might be small.

It is also possible that the ^{10}Be rates are strongly, or systematically, affected by river transience given the evidence for discrete capture of rivers from the high plateau. If the escarpment is retreating through a series of discrete captures, the basin-averaged erosion rate will be cyclic through the process of capture, equilibration and relative stasis prior to the next capture. We cannot easily predict the rates or timescale of that cycle, but it is possible that the overall bias is downward if the cycle is not symmetric with a long period of stasis leading up to the next capture.

Confirmational dating of escarpment retreat is difficult to obtain. Dating of laterites on the coastal plain can be used as a minimum age for the passage of an escarpment. The coastal plain of western India has deep weathering profiles, but most laterite dating has been done on the plateau (Beauvais et al., 2016; Bonnet et al., 2014, 2016). An age of 47 Ma was obtained from K-Mn oxides in an ore pit that is approximately 10 km away from the

escarpment toe of the northern Western Ghats (Beauvais et al., 2016) providing a retreat rate of ~0.2 km/Ma for the time interval of 47 Ma to the present. This rate is consistent with its distance from the coastline. A second age of 27 Ma was obtained nearby, but showed signs of secondary weathering, so provided only a minimum age (Beauvais et al., 2016).

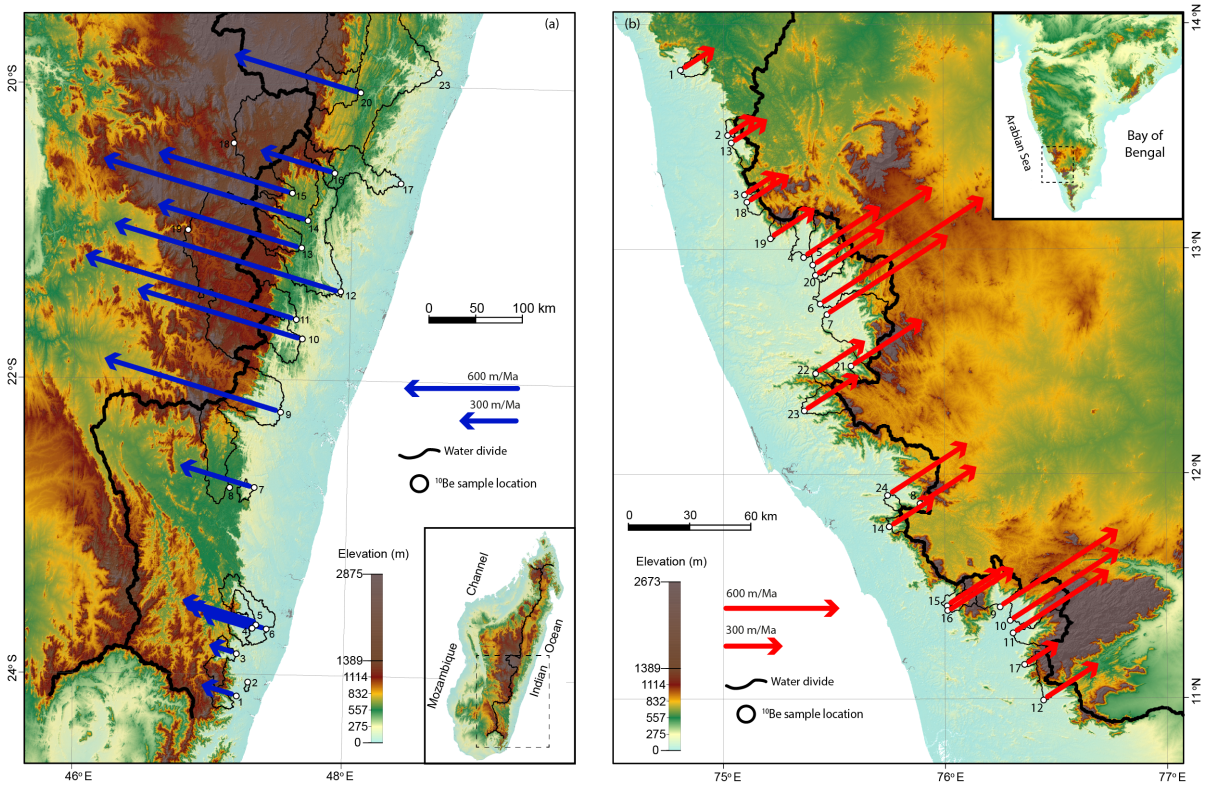

Figure 11. Retreat rates of (a) Madagascar (b) Western Ghats, India, calculated with identical methodology. All quantities are corrected for plateau area and flexural compensation (T_e = 20 km). Continental water divide is shown as thick black lines. Numbers nearby ^{10}Be sample locations on the figure index to respective basins in Table 2-3 and Supplement Table S1.

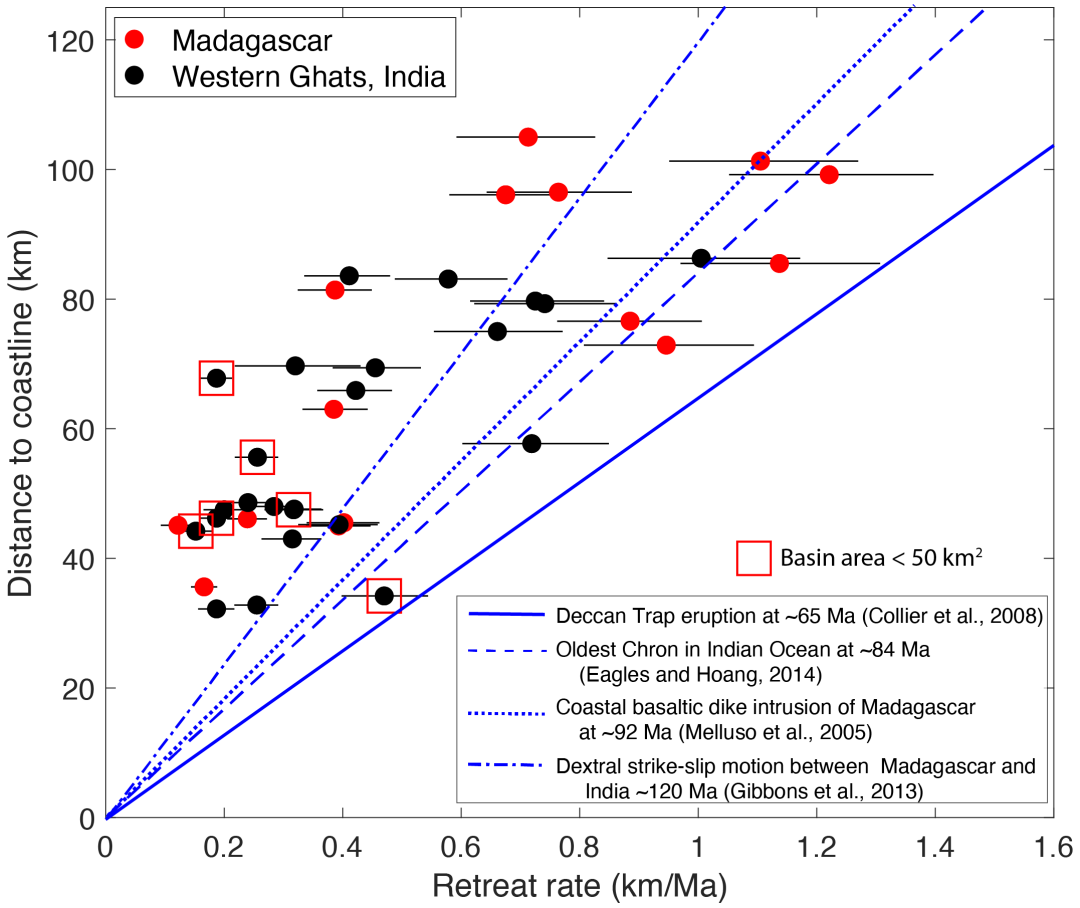

Figure 12. Inferred retreat rate of Madagascar escarpment basins from DCN ^{10}Be concentrations against current distance from the coastline. Retreat rates of Madagascar escarpment are calculated using the Basin Projection method with azimuth taken as N73W. Age of rifting is constrained by various events as indicated and is expected to be older than these constraints. The retreat rates of Madagascar and Western Ghats are corrected for the plateau area from Equation (4) and flexural uplift from Equation (5) for lithosphere elastic thickness of 20 km. See Table 3 for the data.

5.3 Escarpment retreat or vertical uplift?

The prevalent view of a migrating escarpment is that it represents a water divide, perhaps localized by flexural uplift, but migrating inland with the steepest reaches being at or near the water divide (Willett et al., 2019; Braun, 2018; Tucker and Slingerland, 1994; Kooi and Beaumont, 1994). As an escarpment migrates, it has the potential to capture plateau rivers, though the size and frequency of these captures depend on the morphology of the plateau river network (Scheingross et al., 2020; Prince et al., 2010). Captures of plateau rivers by a Type A escarpment river will form a Type B escarpment river (Giachetta and Willett, 2018) where the captured plateau river is the low steepness upper reach on a Type B river profile. Type B escarpment rivers make up 60% of the escarpment rivers in our study area, suggesting that these small-scale capture events are extremely common. Further evidence that this morphology is the response of capture includes the low-gradients of the plateau rivers and the occurrence of barbed tributaries. River valleys of these plateau-flowing reaches near the water divide are typically wide and low-gradient suggesting insufficient sediment

transport and erosional power. In addition, low-elevation windgaps are frequent phenomena at the water divide.

It is also possible that the high frequency of type B rivers along the Madagascar escarpment is due to a nearly continuous migration of this morphology into the plateau. Harel at al. (2019) demonstrated a mechanism of divide migration by progressive reversal of a plateau river after capture by an escarpment river. In this model, the water divide and the escarpment are independent morphologic features, but migrate together and at similar rates. Upland river capture thus becomes a more continuous process rather than a series of discrete, transient events. The large frequency of Type B escarpment rivers suggests that this mechanism might be common in Madagascar. Although Harel et al. (2019) called on easily eroded alluvium for their model, we expect that the common lateritic surface layer of Madagascar could serve the same role and its common presence would explain why the water divide precedes the escarpment so frequently.

River captures occur at many scales in Madagascar. For example, the Mananara river in our study area (Supplement Figure S1), currently drains 1485 km^2 of the highlands to the east coast. Many of the major tributaries of the Mananara are barbed, flowing to the northwest for up to 200 kms before reversing to flow to the east over the escarpment and coastal plain. Schreurs et al. (2009) used this and other evidence to identify this as a major capture event and we would argue that it follows the Harel et al. (2019) model of a reversed trunk reach and captured, barbed tributaries, but at a scale of hundreds of kilometers.

As an alternative to the migrating escarpment model for Madagascar, a number of studies have suggested that the modern topography is the result of Cenozoic uplift. Based on river profile inversion models, Roberts et al. (2012) and Stephenson et al. (2021) proposed that the high topography of central Madagascar plateau formed in the late Cenozoic from accelerating uplift initiating between ~15 Ma to ~30 Ma. Based on the identification of pediment surfaces, Delaunay (2018) proposed that the plateau has undergone episodic uplift since the Cretaceous with the stepped topography established since the rifting of eastern Madagascar with Seychelles-India. The cumulative Cenozoic uplift of the Madagascar plateau is predicted to be 1-2 km from river inversion models (Roberts et al., 2012; Stephenson et al., 2021) and the pediment surface study of Delaunay (2018). Our escarpment retreat model suggests that the rate of retreat is consistent with slow retreat since the Cretaceous rifting, and so, although it does not preclude younger uplift, recent or episodic uplift is not needed to explain the stepped nature of the east-draining rivers or the kilometer-scale topography. We would argue that the current morphology and the ^{10}Be concentrations are consistent with the major topographic uplift being Cretaceous. The regions of western Madagascar that were covered in marine sediments have experienced some additional uplift since deposition, but this need be no more than 1 km to explain the occurrence of marine sediments at elevation.

Vertical uplift and horizontal escarpment retreat into a pre-existing topography represent alternative models, based on different assumptions. The main difference between these models is the assumption regarding drainage basin stability. A retreating escarpment implies continuous divide migration and time-dependent drainage area, whereas river profile analysis explicitly assumes that drainage area and drainage basin geometry remain constant in time.

We suggest several tests to differentiate between these models of landscape evolution. First, is the consistency of river profiles. With vertical uplift and a static geometry to river basin geometry, all river profiles with a common uplift history should exhibit common form once transformed to χ-space (Willett et al., 2014). This is only true for channels with a

common uplift history, but in a tectonically inactive area such as Madagascar, rock uplift is restricted to long wavelength dynamic topography originating in the mantle. Single catchments or neighboring catchments are expected to have a common uplift history. This is particularly true for branches of a single catchment where profile variability due to variations in uplift rate, rock erodibility or precipitation must originate above the common confluence. As shown in Figure 6 and the examples in the supplement (Figure S1-S5) channel profiles exhibit large variability, even within single catchments. In many catchments, the large knickzones defining the escarpment are present in only a fraction of the channels with a large number showing no knickpoint at all (our type A vs. Type B). This is not consistent with the idea of a common uplift history, but is consistent with lateral retreat of the escarpment, with morphological differences being the result of episodic river capture, as well as transients associated with the direction and magnitude of retreat.

The second test we can consider is an analysis of the timescale of landscape response calibrated to our ^{10}Be concentration data. Analysis of river steepness or channel profiles, including inversion of full channel profiles do not contain any information regarding the timescale of transient response. Time information comes through the erodibility parameter, K in the stream power model used in these analyses. Cosmogenic concentration data can provide an estimate of K and timescale information.

The timescale for a river channel to respond to a baselevel change is (Whipple and Tucker, 1999):

$$\tau = \frac{1}{K}\int_0^{x^*} \frac{dx}{A(x)^{\frac{m}{n}}} \quad (6)$$

Where τ is referred to as the response time of an uplift signal to propagate upstream from baselevel to a position x^*along the river, and depends on the erodibility, K, and the exponents, m and n, of the stream power equation. Defining the basin mean normalized steepness index, k_{sn} (Hilley et al., 2019; Wobus et al., 2006), this can be compared to the basin mean erosion rate (e) from the ^{10}Be concentrations to give an estimate of K through the relationship:

$$k_{sn} = \left(\frac{e}{K}\right)^{1/n} \quad (7)$$

Normalized steepness requires an assumption for the ratio of m/n and Equation (7) requires selecting or inferring a value of n. We assumed n=1 and estimated K for two values of m. The ^{10}Be concentrations and the normalized steepness indices are correlated, but not well, implying a wide range of erodibility values or strong disequilibrium in channel profiles which produces variance in the estimation of basin mean steepness (Figure 13). We find a range of K of 1.0×10^{-6} to 3.0×10^{-6}m$^{0.3}$/yr and 0.2×10^{-6} to 0.6×10^{-6} m$^{0.1}$/yr with m=0.35 and 0.45, respectively (Figure 13). There are 3 to 5 very low values of K that might be considered outliers (Figure 13). If we ignore the outliers and regress the remaining data with a concavity of 0.45, we obtain a K of 0.4×10^{-6} m$^{0.1}$/yr (Figure 13b), close to the independent estimate of 0.24×10^{-6} m$^{0.1}$/yr in similar lithology in western India (Mandal et al., 2015). The response time for the landscape with these values of K are shown in Figure 14. Although the range of possible timescales is large, the timescales are long relative to the Cenozoic. For many

acceptable values of K, the equilibration timescale is longer than the time since rifting. This suggests that in the absence of changes in drainage basin geometry, most of the topography would still be unequilibrated to uplift associated with rifting, with no need for Cenozoic uplift. Again, this does not preclude Cenozoic uplift, it simply shows that it is not necessary.

Stephenson (2019) assumed an n=1, m=0.35 and subsequently estimated K=4.2×10^{-6} m$^{0.3}$/yr based on the elevation of uplifted marine sediments. Roberts et al. (2012) assumed n=1, m=0.2 and calculated K =2×10^{-4} m$^{0.6}$/yr from observations of Miocene marine formations that are currently ~ 1 km in elevation. These values of K are higher than our estimate, which greatly reduces the response time of the landscape. The implication is that if our ^{10}Be data correctly characterizes the erosion rates, and the drainage morphology is fixed in time, the response time for the landscape would be much longer than the 30 Ma suggested by both Roberts et al. (2012), Stephenson (2019) and Stephenson et al. (2021) and calibrations to sediment fluxes are offset by a factor of 2 or more.

However, although this is a useful exercise to demonstrate the problematic nature of fixed basin geometry models and vertical uplift, we do not have much confidence in the channel steepness calculations. The transience in river profiles and the intra-basinal variance in channel profiles in response to divide migration is too large to make this calculation accurately. Nor does it accurately reflect the physical morphology, where the escarpment retreat affects concavity which is impossible to differentiate from continuous variation in steepness (Willett et al., 2018).

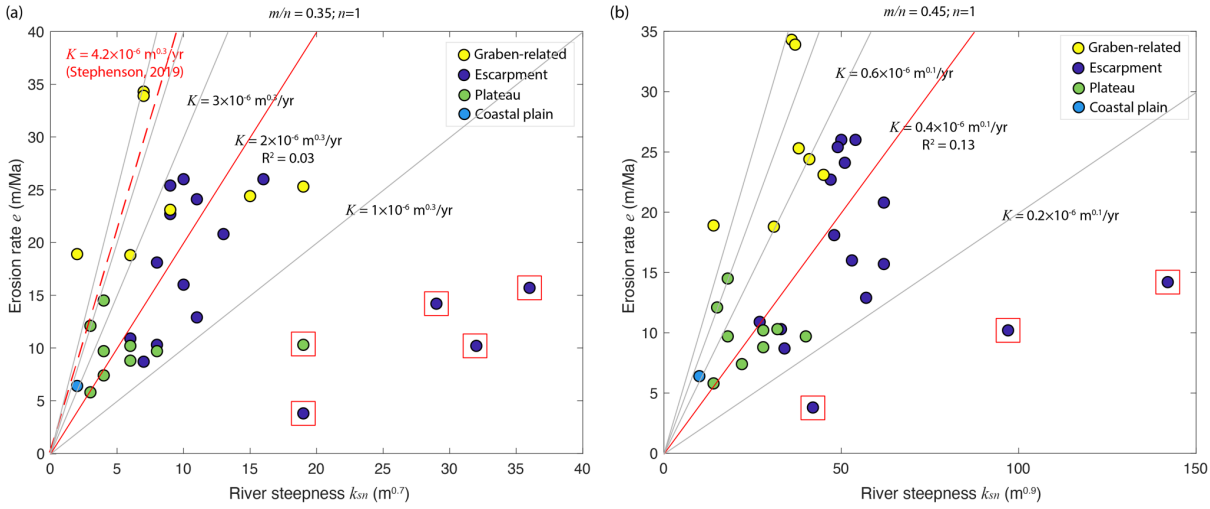

Figure 13. Estimate of erodibility constant K from normalized channel steepness index (k_{sn}) and cosmogenic ^{10}Be-derived basin-averaged erosion rate (e) of Madagascar based on Equation (7). The slope exponent n=1, area exponent (a) m=0.35 and (b) m=0.45. Indeterminate outlier data points are indicated with additional red squares. The red solid lines are regressions of data without the outliers. Solid grey lines show values of K increasing at equal intervals that bracket data. The red dashed line shows the K from Stephenson (2019).

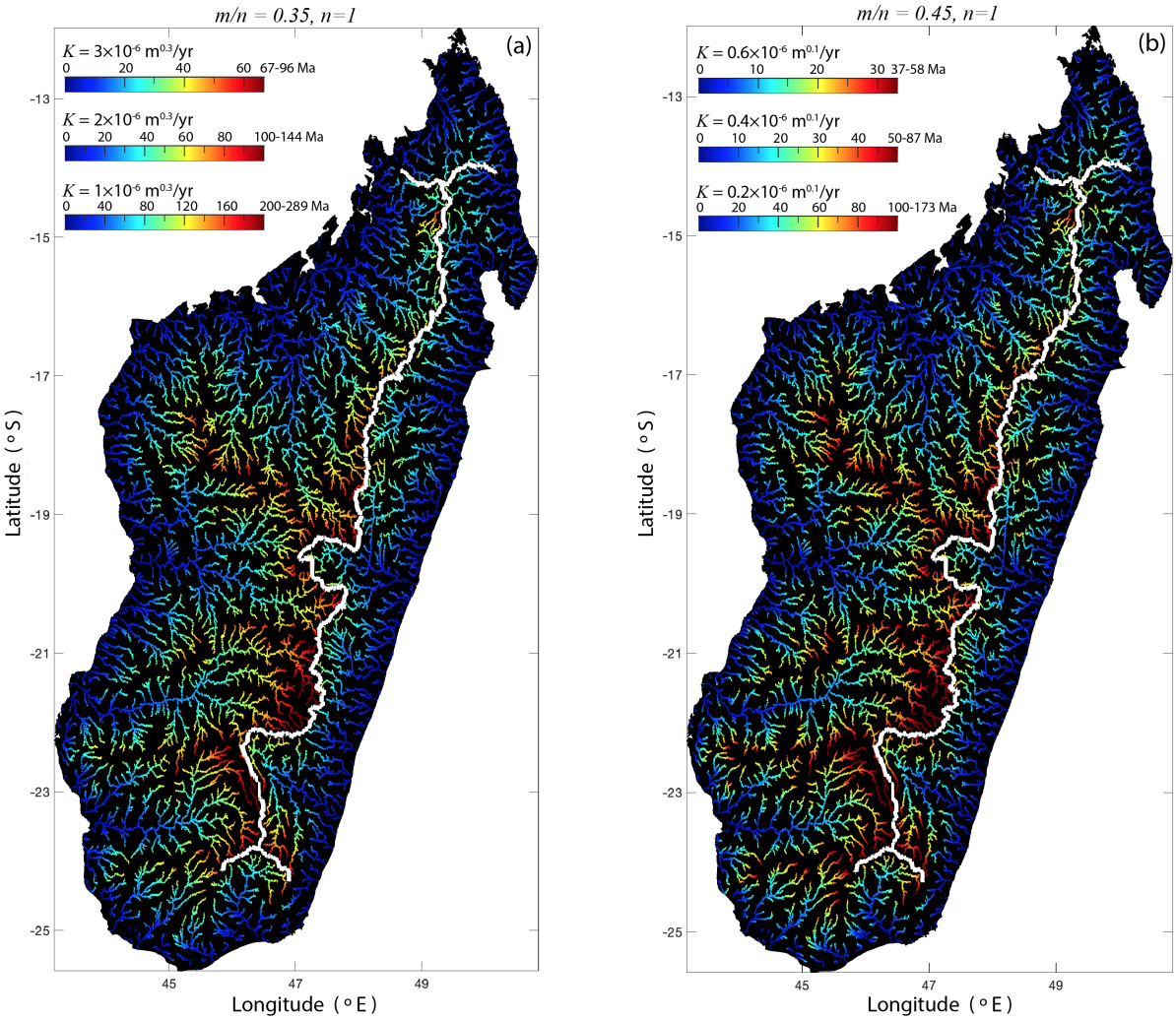

Figure 14. Response time τ of Madagascar rivers for (a) m/n=0.35 and (b) m/n = 0.45 for various K. Rivers are picked with a drainage area larger than 64 km^2. The thick white line shows the continental water divide that separates the eastern escarpment drainages and the western drainages.

6 Conclusions

This study has systematically investigated the erosional fluxes and landscape evolution of the Madagascar escarpment. New DCN ^{10}Be concentration-derived erosion rates reveal differential erosion rates among the three geomorphic zones: the erosion rates of the plateau and the coastal plain have exceptionally low erosion rates averaging only 9.7 m/Ma. Erosion rates are higher on the escarpment front and an average erosion rate of 16.6 m/Ma is calculated for escarpment-draining basins. The active Alaotra-Ankay Graben basins have the highest erosion rates in our study area, with an average rate of 27 m/Ma.

Although the erosion rates are low, the same ^{10}Be concentrations imply retreat of the Madagascar escarpment at rates over an order of magnitude higher. Retreat rates inferred from DCN ^{10}Be concentrations of Madagascar are between 182 m/Ma-1886 m/Ma. These rates are consistent with the distance from the coastline and an average retreat rate since rifting. Landscape evolution dominated by escarpment retreat is consistent with the asymmetric morphology of Madagascar, geomorphic variance of river profiles and other

728 features characteristic of frequent river capture. We conclude that the landscape evolution of
729 Madagascar, and by analogy, the Western Ghats and other passive margin escarpments, are
730 dominated by escarpment retreat, drainage basin growth and reorganization and little uplift or
731 erosion of pre-existing highlands since rifting.

732

733 **References**

734 Andriampenomanana, F., Nyblade, A. A., Wysession, M. E., Durrheim, R. J., Tilmann, F.,
735 Julia, J., . . . others (2017). The structure of the crust and uppermost mantle beneath
736 madagascar. Geophysical Journal International, 210 (3), 1525-1544.
737 doi:10.1093/gji/ggx243

738 Balco, G., Stone, J. O., Lifton, N. A., & Dunai, T. J. (2008). A complete and easily accessible
739 means of calculating surface exposure ages or erosion rates from 10be and 26al
740 measurements. Quaternary geochronology, 3 (3), 174-195.
741 doi:10.1016/j.quageo.2007.12.001

742 Beauvais, A., Bonnet, N. J., Chardon, D., Arnaud, N., & Jayananda, M. (2016). Very long-
743 term stability of passive margin escarpment constrained by 40ar/39ar dating of k-mn
744 oxides. Geology, 44 (4), 299-302. doi:10.1130/G37303.1

745 Bonnet, N. J., Beauvais, A., Arnaud, N., Chardon, D., & Jayananda, M. (2014). First
746 40ar/39ar dating of intense late palaeogene lateritic weathering in peninsular India.
747 Earth and Planetary Science Letters, 386 , 126-137. doi:10.1016/j.epsl.2013.11.002

748 Bonnet, N. J., Beauvais, A., Arnaud, N., Chardon, D., & Jayananda, M. (2016). Cenozoic
749 lateritic weathering and erosion history of peninsular India from 40ar/39ar dating of
750 supergene k-mn oxides. Chemical Geology, 446 , 33-53.
751 doi:10.1016/j.chemgeo.2016.04.018

752 Braucher, R., Merchel, S., Borgomano, J., & Bourlès, D. (2011). Production of cosmogenic
753 radionuclides at great depth: A multi element approach. Earth and Planetary Science
754 Letters, 309 (1-2), 1-9. doi:10.1016/j.epsl.2011.06.036

755 Braun, J. (2018). A review of numerical modeling studies of passive margin escarpments
756 leading to a new analytical expression for the rate of escarpment migration velocity.
757 Gondwana Research, 53 , 209-224. doi:10.1016/j.gr.2017.04.012

758 Chmeleff, J., von Blanckenburg, F., Kossert, K., & Jakob, D. (2010). Determination of the
759 10be half-life by multicollector icp-ms and liquid scintillation counting. Nuclear
760 Instruments and Methods in Physics Research Section B: Beam Interactions with
761 Materials and Atoms, 268 (2), 192-199. doi:10.1016/j.nimb.2009.09.012

762 Christl, M., Vockenhuber, C., Kubik, P. W., Wacker, L., Lachner, J., Alfimov, V., & Synal,
763 H.-A. (2013). The ETH Zurich AMS facilities: Performance parameters and reference
764 materials. Nuclear Instruments and Methods in Physics Research Section B: Beam
765 Interactions with Materials and Atoms, 294 , 29-38. doi:10.1016/j.nimb.2012.03.004

766 Collier, J., Sansom, V., Ishizuka, O., Taylor, R., Minshull, T., & Whitmarsh, R. (2008). Age
767 of Seychelles-india break-up. Earth and Planetary Science Letters, 272 (1-2), 264-
768 277. doi:10.1016/j.epsl.2008.04.045

769 Cox, R., Bierman, P., Jungers, M. C., & Rakotondrazafy, A. M. (2009). Erosion rates and
770 sediment sources in Madagascar inferred from 10be analysis of lavaka, slope, and
771 river sediment. The Journal of Geology, 117 (4), 363-376. doi:10.1086/598945

772 Cox, R., Zentner, D. B., Rakotondrazafy, A. F. M., & Rasoazanamparany, C. F. (2010).
773 Shakedown in Madagascar: Occurrence of lavakas (erosional gullies) associated with
774 seismic activity. Geology, 38 (2), 179-182. doi:10.1130/G30670.1

775 Delaunay, A. (2018). The vertical movements of madagascar (90-0 ma): a coupled analysis
776 of the landforms and the dimentional recording of the western Malagasy margins
777 (Unpublished doctoral dissertation). Rennes 1.

778 DiBiase, R. A. (2018). Increasing vertical attenuation length of cosmogenic nuclide
779 production on steep slopes negates topographic shielding corrections for catchment
780 erosion rates. Earth Surface Dynamics, 6 (4), 923-931. doi: 10.5194/esurf-6-923-2018

781 Eagles, G., & Hoang, H. H. (2014). Cretaceous to present kinematics of the Indian, African
782 and Seychelles plates. Geophysical Journal International, 196 (1), 1-14.
783 doi:10.1093/gji/ggt372

784 Emmel, B., Boger, S., Jacobs, J., & Daszinnies, M. (2012). Maturity of central Madagascar's
785 landscape low-temperature thermochronological constraints. Gondwana Research, 21
786 (2-3), 704-713. doi:10.1016/j.gr.2011.05.018

787 Giachetta, E., & Willett, S. D. (2018). Effects of river capture and sediment flux on the
788 evolution of plateaus: insights from numerical modeling and river profile analysis in
789 the upper blue Nile catchment. Journal of Geophysical Research: Earth Surface, 123
790 (6), 1187-1217. doi:10.1029/2017JF004252

791 Gibbons, A. D., Whittaker, J. M., & Muller, R. D. (2013). The breakup of east Gondwana:
792 Assimilating constraints from cretaceous ocean basins around India into a best-fit
793 tectonic model. Journal of geophysical research: solid earth, 118 (3), 808-822.
794 doi:10.1002/jgrb.50079

795 Godard, V., Dosseto, A., Fleury, J., Bellier, O., Siame, L., Team, A., et al. (2019). Transient
796 landscape dynamics across the southeastern Australian escarpment. Earth and
797 Planetary Science Letters, 506 , 397-406. doi:10.1016/j.epsl.2018.11.017

798 Gunnell, Y., & Harbor, D. (2008). Structural underprint and tectonic overprint in the Angavo
799 (Madagascar) and western ghats (india)-implications for understanding scarp
800 evolution at passive margins. JOURNAL GEOLOGICAL SOCIETY OF INDIA, 71
801 (6), 763. Retrieved from
802 http://www.geosocindia.org/index.php/jgsi/article/view/80750

803 Gunnell, Y., & Harbor, D. (2010). Butte detachment: how pre-rift geological structure and
804 drainage integration drive escarpment evolution at rifted continental margins. Earth
805 Surface Processes and Landforms, 35 (12), 1373-1385. doi:10.1002/esp.1973

806 Harel, E., Goren, L., Shelef, E., & Ginat, H. (2019). Drainage reversal toward cliffs induced
807 by lateral lithologic differences. Geology, 47 (10), 928-932. doi:10.1130/G46353.1

808 Hilley, G. E., Porder, S., Aron, F., Baden, C. W., Johnstone, S. A., Liu, F., . . .Young, H. H.
809 (2019). Earths topographic relief potentially limited by an upper bound on channel
810 steepness. Nature Geoscience, 12 (10), 828-832. doi:10.1038/s41561-019-0442-3

811 Jarvis, A., Reuter, H., Nelson, A., & Guevara, E. (2008). Hole-filled seamless SRTM data,
812 version 4, international centre for tropical agriculture (ciat). Retrieved from
813 http://srtm.csi.cgiar.org

814 Kirby, E., & Whipple, K. X. (2012). Expression of active tectonics in erosional landscapes.
815 Journal of Structural Geology, 44 , 54-75. doi:10.1016/j.jsg.2012.07.009

816 Kooi, H., & Beaumont, C. (1994). Escarpment evolution on high-elevation rifted margins:
817 Insights derived from a surface processes model that combines diffusion, advection,
818 and reaction. Journal of Geophysical Research: Solid Earth, 99 (B6), 12191-12209.
819 doi:10.1029/94JB00047

820 Kusky, T. M., Toraman, E., Raharimahefa, T., & Rasoazanamparany, C. (2010). Active
821 tectonics of the Alaotra-Ankay graben system, Madagascar: possible extension of
822 Somalian-African diffusive plate boundary? Gondwana Research, 18 (2-3), 274-294.
823 doi:10.1016/j.gr.2010.02.003

824 Lupker, M., Blard, P.-H., Lave, J., France-Lanord, C., Leanni, L., Puchol, N., . . .Bourles, D.
825 (2012). 10be-derived himalayan denudation rates and sediment budgets in the ganga
826 basin. Earth and Planetary Science Letters, 333 , 146-156.
827 doi:10.1016/j.epsl.2012.04.020

828 Mandal, S. K., Lupker, M., Burg, J.-P., Valla, P. G., Haghipour, N., & Christl, M. (2015).
829 Spatial variability of 10be-derived erosion rates across the southern peninsular indian
830 escarpment: A key to landscape evolution across passive margins. Earth and Planetary
831 Science Letters, 425 , 154-167. doi:10.1016/j.epsl.2015.05.050

832 Matmon, A., Bierman, P., & Enzel, Y. (2002). Pattern and tempo of great escarpment
833 erosion. Geology, 30 (12), 1135-1138.
834 doi:10.1130/00917613(2002)030h1135:PATOGEi2.0.CO;2

835 Melluso, L., Morra, V., Brotzu, P., Tommasini, S., Renna, M. R., Duncan, R. A.,. . .
836 D'AMELIO, F. (2005). Geochronology and petrogenesis of the Cretaceous
837 Antampombato-Ambatovy complex and associated dyke swarm, Madagascar. Journal
838 of Petrology, 46 (10), 1963-1996. doi:10.1093/petrology/egi044

839 Nassor, A., & Jury, M. (1998). Intra-seasonal climate variability of madagascar. part 1: Mean
840 summer conditions. Meteorology and Atmospheric Physics, 65 (1), 31-41.
841 doi:10.1007/BF01030267

842 Ochs, S. D. I. (1996). The dating of rock surfaces using in situ produced 10ae, 26 al and 36ci,
843 with examples from antarctica and the swiss alps (Doctoral dissertation, ETH Zurich,
844 Zurich). doi:10.3929/ethz-a-001772745

845 Ohba, M., Samonds, K. E., LaFleur, M., Ali, J. R., & Godfrey, L. R. (2016). Madagascar's
846 climate at the k/p boundary and its impact on the island's biotic suite.
847 Palaeogeography, Palaeoclimatology, Palaeoecology, 441 , 688-695.
848 doi:10.1016/j.palaeo.2015.10.028

849 Perron, J.T. and Royden, L. (2013), An integral approach to bedrock river profile analysis.
850 Earth Surf. Process. Landforms, 38: 570-576. doi:10.1002/esp.3302

851 Pratt, M. J., Wysession, M. E., Aleqabi, G., Wiens, D. A., Nyblade, A. A., Shore, P., . . .
852 others (2017). Shear velocity structure of the crust and upper mantle of Madagascar
853 derived from surface wave tomography. Earth and Planetary Science Letters, 458 ,
854 405-417. doi:10.1016/j.epsl.2016.10.041

855 Prince, P. S., Spotila, J. A., & Henika, W. S. (2010). New physical evidence of the role of
856 stream capture in active retreat of the blue ridge escarpment, southern appalachians.
857 Geomorphology, 123 (3-4), 305-319. doi:10.1016/j.geomorph.2010.07.023

858 Roberts, G. G., Paul, J. D., White, N., & Winterbourne, J. (2012). Temporal and spatial
859 evolution of dynamic support from river profiles: A framework for Madagascar.
860 Geochemistry, Geophysics, Geosystems, 13 (4). doi:10.1029/2012GC004040

Roig, J., Tucker, R., Delor, C., Peters, S., & Th 'e veniaut, H. (2012). Map g 'eologique de la r e publique de madagascar `a 1 / 1,000,000 ministe re des mines, program de gouvernance des ressources min 'e rales. R 'e publique de Madagascar, Antananarivo.

Salgado, A. A., Marent, B. R., Cherem, L. F., Bourles, D., Santos, L. J., Braucher, R., & Barreto, H. N. (2014). Denudation and retreat of the serra do mar escarpment in southern brazil derived from in situ-produced 10be concentration in river sediment. Earth Surface Processes and Landforms, 39 (3), 311-319. doi:10.1002/esp.3448

Scheingross, J. S., Limaye, A. B., McCoy, S. W., & Whittaker, A. C. (2020). The shaping of erosional landscapes by internal dynamics. Nature Reviews Earth & Environment, 1-16. doi:10.1038/s43017-020-0096-0

Schettino, A., & Scotese, C. R. (2005). Apparent polar wander paths for the major continents (200 ma to the present day): a palaeomagnetic reference frame for global plate tectonic reconstructions. Geophysical Journal International, 163 (2), 727-759. doi:10.1111/j.1365-246X.2005.02638.x

Schreurs, G., Giese, J., Berger, A., & Gnos, E. (2010). A new perspective on the signi_cance of the ranotsara shear zone in madagascar. International journal of earth sciences, 99 (8), 1827-1847. doi:10.1007/s00531-009-0490-9

Scroxton, N., Burns, S. J., McGee, D., Hardt, B., Godfrey, L. R., Ranivoharimanana, L., & Faina, P. (2017). Hemispherically in-phase precipitation variability over the last 1700 years in a madagascar speleothem record. Quaternary Science Reviews, 164 , 25-36. doi:10.1016/j.quascirev.2017.03.017

Stephenson, S. (2019). Dynamic topography of madagascar and its surroundings (Doctoral dissertation, University of Cambridge). doi:10.17863/CAM.38636

Stephenson, S. N., White, N., Carter, A., Seward, D., Ball, P., & Klocking, M.(2021). Cenozoic dynamic topography of madagascar. Geochemistry, Geophysics, Geosystems, e2020GC009624. doi:10.1029/2020GC009624

Stephenson, S. N., White, N. J., Li, T., & Robinson, L. F. (2019). Disentangling interglacial sea level and global dynamic topography: analysis of Madagascar. Earth and Planetary Science Letters, 519 , 61-69. doi:10.1016/j.epsl.2019.04.029

Stone, J. O. (2000). Air pressure and cosmogenic isotope production. Journal of Geophysical Research: Solid Earth, 105 (B10), 23753-23759. doi:10.1029/2000JB900181

Torsvik, T., Tucker, R., Ashwal, L., Eide, E., Rakotosolofo, N., & De Wit, M. (1998). Late cretaceous magmatism in madagascar: palaeomagnetic evidence for a stationary marion hotspot. Earth and Planetary Science Letters, 164 (1-2), 221-232. doi:10.1016/S0012-821X(98)00206-4

Tucker, G. E., & Slingerland, R. L. (1994). Erosional dynamics, flexural isostasy, and long-lived escarpments: A numerical modeling study. Journal of Geophysical Research: Solid Earth, 99 (B6), 12229-12243. doi:10.1029/94JB00320

Turcotte, D., & Schubert, G. (2002). Geodynamics, chapter 3: Elasticity and Cambridge University Press. doi:10.1017/CBO9780511807442.005

Voarintsoa, N., Cox, R., Razanatseheno, M., & Rakotondrazafy, A. (2012). Relation between bedrock geology, topography and lavaka distribution in Madagascar. South African Journal of Geology, 115 (2), 225-250. doi:10.2113/gssajg.115.225

Von Blanckenburg, F. (2005). The control mechanisms of erosion and weathering at basin scale from cosmogenic nuclides in river sediment. Earth and Planetary Science Letters, 237 (3-4), 462-479. doi:10.1016/j.epsl.2005.06.030

Wang, Y., & Willett, S. (2021). Escarpment retreat rates derived from detrital cosmogenic nuclide concentrations. Earth Surface Dynamics Discussions [preprint], 1-38. doi:10.5194/esurf-2021-27

Wells, N., Andriamihaja, B., Goodman, S., & Patterson, B. (1997). Extreme gully erosion in madagascar and its natural and anthropogenic causes. Natural change and human impact in Madagascar, 44-47.

Wells, N. A., & Andriamihaja, B. (1990). Evidence for cryptic colluvial addition and removal at the tops of laterite profiles in madagascar/mise en evidence d'apport et d'ablation de colluvions cryptiques au sommet de profils lateritiques de madagascar. Sciences Geologiques, bulletins et memoires, 43 (2), 237-251. doi:10.3406/sgeo;/1990.1858

Whipple, K. X., & Tucker, G. E. (1999). Dynamics of the stream-power river incision model: Implications for height limits of mountain ranges, landscape response timescales, and research needs. Journal of Geophysical Research: Solid Earth, 104(B8), 17661-17674. doi : 10.1029/1999jb900120

Willett, S. D., McCoy, S. W., & Beeson, H. W. (2018). Transience of the north American high plains landscape and its impact on surface water. Nature, 561 (7724), 528-532. doi:10.1038/s41586-018-0532-1

Willett, S. D., McCoy, S. W., Perron, J. T., Goren, L., & Chen, C. Y. (2014). Dynamic reorganization of river basins. Science, 343(6175). doi: 10.1126/science.1248765

Wit, M. J. d. (2003). Madagascar: heads its a continent, tails its an island. Annual Review of Earth and Planetary Sciences, 31 (1), 213-248. doi:10.1146/annurev.earth.31.100901.141337

Wobus, C., K. X. Whipple, E. Kirby, N. Snyder, J. Johnson, K. Spyropolou, B. Crosby, and D. Sheehan (2006), Tectonics from topography: Procedures, promise, and pitfalls, Geological Society of America, Special Papers, 398, 55– 74, doi:10.1130/2006.2398(04).